NASA Technical Paper 2940

November 1989

Analysis of Flight Data From a High-Incidence Research Model by System Identification Methods

(NASA-TP-2940) ANALYSIS OF FLIGHT DATA FROM A HIGH-INCIDENCE RESEARCH MODEL BY SYSTEM IDENTIFICATION METHODS (NASA. Langley Research Center) 50 p

N90-10074

CSCL 01C

Unclas

H1/08 0222558

James G. Batterson
and Vladislav Klein

NASA

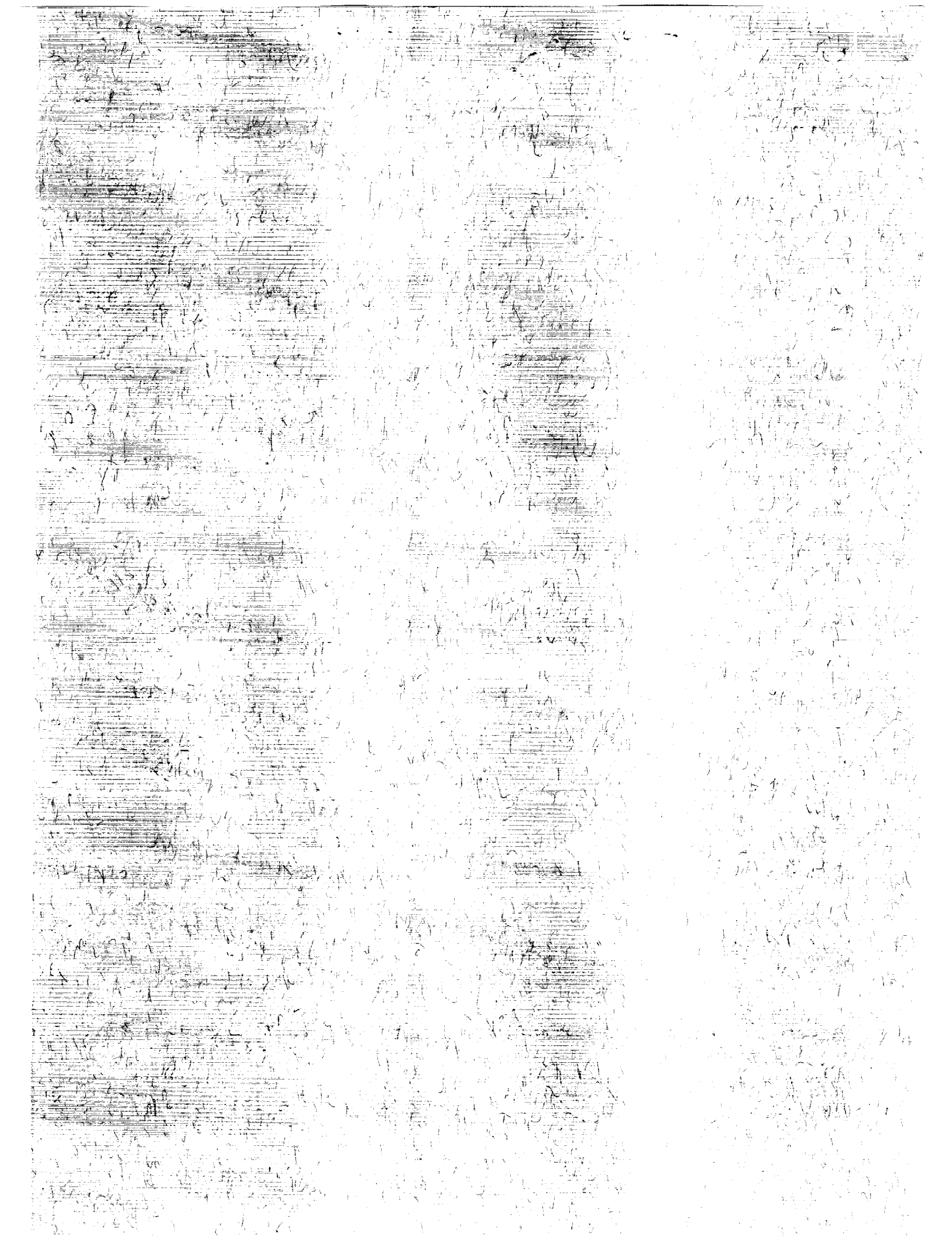

NASA Technical Paper 2940

1989

Analysis of Flight Data From a High-Incidence Research Model by System Identification Methods

James G. Batterson
Langley Research Center
Hampton, Virginia

Vladislav Klein
The George Washington University
Joint Institute for Advancement of Flight Sciences
Langley Research Center
Hampton, Virginia

National Aeronautics and Space Administration
Office of Management
Scientific and Technical Information Division

Summary

Data partitioning and modified stepwise regression were applied to recorded flight data from a Royal Aerospace Establishment (RAE) high-incidence research model (HIRM). An aerodynamic model structure and the corresponding stability and control derivatives were determined for angles of attack between 18° and 30°. Several nonlinearities in angles of attack and sideslip as well as a unique roll-dominated set of lateral modes were found. All flight-estimated values were compared with available wind-tunnel measurements.

Introduction

The Royal Aerospace Establishment (RAE) is currently leading an extensive program of research into the high-angle-of-attack aerodynamic behavior of current and future combat aircraft configurations (ref. 1). The main thrust of the program is to produce an adequate mathematical model of the aircraft aerodynamics at high angles of attack so that control laws can be designed for enhanced maneuverability and departure prevention. The program includes theoretical studies (ref. 2), extensive wind-tunnel testing (refs. 3–6), and flight testing of unpowered drop models (ref. 7). One of the vehicles for investigation is the high-incidence research model (HIRM), a canard/sweptback-wing configuration.

While theoretical analysis, wind-tunnel testing, and short test flights (20 sec or less) are being carried out in the United Kingdom (UK) by the RAE, the responsibility for extended test flights (up to 160 sec) and flight data analysis is shared with the National Aeronautics and Space Administration (NASA) at its Dryden Flight Research Facility (DFRF) and Langley Research Center (LaRC). Flight tests were carried out in 1983 and 1986 under Task 18 of the NASA/RAE Joint Aeronautical Program. As a result of unpredicted, violent wing rock episodes in several of the 1983 flights, Task 32 was added to the joint program for the purpose of determining the cause of that wing rock using LaRC's system identification expertise. DFRF provided flight test support, and LaRC planned the 1986 flight maneuvers and applied its system identification expertise to the acquired flight data from 1983 and 1986 for mathematical modeling. Some results from the analysis of the 1983 series were published previously (ref. 2) and were used to plan the 1986 test program.

The purpose of this report is to present results from the analysis of flight data from both the 1983 and 1986 series. The aim of that analysis was to determine an adequate model of the aerodynamics of the HIRM vehicle in the tested flight regimes. This model should explain all analyzed data and it should also have good prediction capability for data not included in the analysis. In order to obtain an adequate model, three procedural steps were taken: (1) data were partitioned into subsets, each comprising a small angle-of-attack range; (2) stepwise regression was applied to each subset to determine model structure and stability and control derivatives; and (3) additional research flights were designed and flown, and steps 1 and 2 were applied to them. The results are mainly in the form of body-axis stability and control derivatives. This report will include a sample of flight data time histories, a discussion of the data analysis techniques, and all the results obtained from applying those techniques to the flight data. All results will be compared with available wind-tunnel data. The report is organized as follows: After this introduction, the flight vehicle, flight tests, and flight data will be discussed. Next, available wind-tunnel data will be summarized and flight data analysis methods will be presented. The main results of the data analysis follow, and a concluding section summarizes the results and provides suggestions for further work.

Symbols

Values are given in SI Units, but they are occasionally given in U.S. Customary Units where considered useful. Measurements and calculations were made in SI Units.

a_x, a_y, a_z	longitudinal, lateral, and vertical accelerations, respectively, g units
b	wing span, m
C_a	general aerodynamic force and moment coefficient
C_L	lift coefficient, $L/\bar{q}S$
C_l	rolling-moment coefficient, $M_X/\bar{q}Sb$
C_m	pitching-moment coefficient, $M_Y/\bar{q}S\bar{c}$
C_n	yawing-moment coefficient, $M_Z/\bar{q}Sb$
C_X	longitudinal-force coefficient, $F_X/\bar{q}S$
C_Y	lateral-force coefficient, $F_Y/\bar{q}S$
C_Z	vertical-force coefficient, $F_Z/\bar{q}S$
$\bar{c}$	wing mean aerodynamic chord, m

F	statistical F-values
F_X, F_Y, F_Z	forces along longitudinal, lateral, and vertical body axes, respectively, N
$f(\ )$	function
g	acceleration due to gravity ($1g \approx 9.81$ m/sec^2), m/sec^2
I_X, I_Y, I_Z	moments of inertia about longitudinal, lateral, and vertical body axes, respectively, kg-m^2
I_{XZ}	product of inertia, kg-m^2
i	$= \sqrt{-1}$
J	cost function
k_D, k_R, k_S	damping factors for Dutch roll, roll, and spiral modes, respectively
k_1, k_2, k_3	damping factor for three lateral modes found in flight data
L	lift force, N
M_X, M_Y, M_Z	rolling, pitching, and yawing moments, N-m
m	mass, kg
N	number of data points
N_{Re}	Reynolds number based on wing reference chord
p	roll rate, rad/sec or deg/sec
q	pitch rate, rad/sec or deg/sec
$\bar{q}$	dynamic pressure, $\frac{1}{2}\rho V^2$, Pa
R^2	square of multiple-correlation coefficient
r	yaw rate, rad/sec or deg/sec
S	wing area, m^2
s^2	residual mean square
t	time, sec
u, v, w	longitudinal, lateral, and vertical airspeed components, respectively, m/sec
V	airspeed, m/sec
$\boldsymbol{X}$	matrix of independent variables
X, Y, Z	longitudinal, lateral, and vertical body axes, respectively
$\boldsymbol{Y}$	vector of measurements of dependent variable
y	dependent variable in regression equation
α	angle of attack, rad or deg
β	sideslip angle, rad or deg
δ_c	symmetric canard deflection, rad or deg
$\delta_{\mathrm{control}}$	any control variable, rad or deg
δ_{cd}	differential canard deflection, rad or deg
δ_d	differential tail deflection, rad or deg
δ_h	symmetric tail deflection, rad or deg
δ_r	rudder deflection, rad or deg
$\boldsymbol{\epsilon}$	equation error vector
$\boldsymbol{\Theta}$	unknown parameter vector
$\boldsymbol{\theta}_i$	stability and control derivative
θ	pitch angle, rad
λ	eigenvalue
ρ	air density, kg/m^3
ν	residual (difference between values of measured and predicted or computed variable)
ϕ	roll angle, rad
Ψ	heading angle, rad
ω	frequency of lateral oscillatory mode from flight data, 1/sec
ω_D	frequency of Dutch roll mode, 1/sec

Abbreviations:

BAe	British Aerospace
c.g.	center of gravity
HIRM	high-incidence research model
MSR	modified stepwise regression
RAE	Royal Aerospace Establishment (formerly Royal Aircraft Establishment)

SAS	stability augmentation system
SR	stepwise regression

A dot $(\cdot)$ over a symbol denotes a derivative with respect to time. A bar $(\bar{})$ over a symbol indicates an average value. A circumflex $(\hat{})$ denotes an estimated value.

Derivatives of the aerodynamic coefficient C_a (where $a = X$, Y, Z, m, l, and n) referenced to a system of body axes with the origin at the airplane center of gravity are given as follows:

$$C_{a_p} = \frac{\partial C_a}{\partial \frac{pb}{2V}} \qquad C_{a_q} = \frac{\partial C_a}{\partial \frac{q\bar{c}}{2V}}$$

$$C_{a_r} = \frac{\partial C_a}{\partial \frac{rb}{2V}} \qquad C_{a_\alpha} = \frac{\partial C_a}{\partial \alpha}$$

$$C_{a_\beta} = \frac{\partial C_a}{\partial \beta} \qquad C_{a_{\beta^3}} = \frac{1}{6}\frac{\partial^3 C_a}{\partial \beta^3}$$

$$C_{a_{\delta d}} = \frac{\partial C_a}{\partial \delta_d} \qquad C_{a_{\delta h}} = \frac{\partial C_a}{\partial \delta_h}$$

Flight Vehicle and Flight Test

HIRM is a three-surface, close-coupled canard/sweptback-wing drop model representative of a class of future fighter aircraft configurations. The canard/swept-wing combination allows for superior transonic performance, and an all-moving tail provides enhanced pitch control. Drawings of the vehicle are presented in figure 1. Geometric, mass, and inertia characteristics (where the c.g. is at 12.5-percent $\bar{c}$) are given in the following table:

Wing area, m^2	2.062
Wing span, m	2.504
Wing mean aerodynamic chord, m	0.868
Mass, kg	248.8
I_X, kg-m^2	17.8
I_Y, kg-m^2	151
I_Z, kg-m^2	164
I_{XZ}, kg-m^2	−0.19

Longitudinal control is achieved by a symmetric canard and all-moving tail (used either separately or together). Lateral-directional control is achieved through the use of a differential canard, differential horizontal tail, and rudder. The flight vehicle was sized so that a full-scale model could be tested in the wind tunnel at flight Reynolds numbers.

Flight instrumentation included three rate gyros, roll and pitch attitude gyros, three linear accelerometers, angle-of-attack and sideslip sensors, and a pitot static probe; potentiometers were installed at each control surface to measure surface deflections. Flight data were telemetered to a ground station and recorded for future processing. There was no ground-to-vehicle radio uplink. Therefore, all flights had to be carefully planned using the best available mathematical model to design a preprogrammed set of control inputs to achieve desired flight test conditions and responses. After a flight had been planned, trim conditions and simple responses were checked in short flights (approximately 20-sec duration) at RAE Larkhill in the UK. The major test flights took place in two series (1983 and 1986) at the NASA Dryden Flight Research Facility (DFRF) in the United States. The flights at DFRF normally lasted between 120 and 140 sec each.

The 1983 series investigated the response of HIRM to differential canard and differential tail doublets and rudder pulses for the two mean canard settings of 0° and −10° and to mean tail settings to trim the vehicle at angles of attack greater than 20°. During several of these flights, a large wing rock type of lateral oscillation occurred spontaneously.

The 1986 series was planned to investigate this wing rock region further as well as test several control laws for departure prevention and for angle-of-attack and bank-angle control. The control laws for departure prevention (DEPS) were formulated to prevent departure from controlled flight by limiting angle of attack. The other set of control laws (HIRM aerodynamic parameter identification, or HAPI) was designed to maintain steady longitudinal flight during lateral responses to yaw and roll control inputs and to prevent excessive bank angles (greater than 30°). Canard settings for the 1986 series were mostly 0° and −5° with some data taken for $\delta_c = -3°$. There were no differential canard inputs designed for system identification; the rudder and differential tail were employed only to control excessive bank angle. Symmetric tail inputs were limited to steps required to change the trim angle of attack.

A typical flight at DFRF began by towing HIRM by helicopter to an altitude of approximately 10 000 ft. The vehicle was then released to glide back to Earth while executing its preprogrammed set of control instructions along with those inputs demanded by the augmentation system. At approximately 1000 ft above ground level, a parachute was deployed to slow the vehicle and lower it to the ground. Air bags were deployed beneath the vehicle to cushion its landing.

Flight Data

Recorded flight data were sent from the Dryden Flight Research Facility to the RAE (at

Farnborough, UK) where they were converted to engineering units and digitized to a time between samples of 0.0116 sec. Those digitized data were then sent to NASA LaRC on several 9-track magnetic tapes for data analysis. Time histories for selected input and response variables are given in figure 2 for the first 35 sec of one of the 1983 flights. The rapid pitch-up and settling out to the trim angle of attack after release from tow (at approximately 2.6 sec) is seen. At approximately 10 sec into the flight, an exaggerated Dutch roll or wing rock type of motion starts to build. The oscillatory motion is disturbed only briefly by the sharp differential tail doublet (originally planned to excite rolling motion for parameter identification) at 23 sec into the flight. For comparison, time histories from the first 40 sec of one of the augmented 1986 flights are given in figure 3. Again, there is a large longitudinal response to the release from the tow line. However, the active augmentation is visible as increased control activity—particularly in differential tail and rudder—to keep the bank angle controlled when changing trim conditions. The continuation of the 1983 flight is given in figure 4 (with a new scale) in which a wing rock spontaneously develops as the trim angle of attack reaches down into the 24° region. The end time of figure 3 and the start time of figure 4 appear to overlap but do not, because figure 3 was shifted 2.6 sec for the purpose of plotting.

The data used in the analysis presented in this paper are drawn from five 1983 flights (RAE designations HD1, HD3, HD5, HD2, and HD4) and from four 1986 flights (HD8, HD19, HAD9, and HAD16). Flights HD1, HD3, and HD5 have −10° canard settings, and flights HD2 and HD4 have a 0° canard setting. For the 1986 series all flights included both 0° and −5° canard settings. Flights HD8 and HD19 were unaugmented, whereas flights HAD9 and HAD16 were augmented.

The 1983 trials contained several well-planned system identification maneuvers in which the vehicle was excited first by the release from the helicopter and then from trim using programmed control inputs. Those control inputs were elevator square-wave doublets designed to excite the short-period longitudinal dynamics of the vehicle and rudder/differential tail square-wave doublet combinations to excite lateral motion. An individual maneuver comprised the input doublet(s) and response to that input. Each of the individual maneuvers was analyzed by itself. The 1986 trials, designed to gently and carefully probe the wing rock regions, had only preprogrammed step inputs of less than 1° from the horizontal stabilator (longitudinal), whereas lateral inputs were initiated only by the flight control system computer as the bank angle approached ±30° or the trim angle of attack was changed. An example of an individual maneuver from the 1983 series is the differential horizontal stabilator doublet shown in figure 5(a). Figure 5(b) shows the type of control surface motion that had to be utilized as initiating an individual maneuver in the 1986 test data.

Wind-Tunnel Tests

The RAE conducted extensive wind-tunnel testing of the HIRM. Data were taken for 0.22-, 0.36-, 0.44-, and full-scale models. Early static tests were conducted on a 0.36-scale preliminary version of HIRM in the RAE (Farnborough) No. 2 $11\frac{1}{2}$- by 8-Foot Tunnel ($0° < \alpha < 40°$) and in the RAE (Bedford) 13- by 9-Foot Tunnel ($0° < \alpha < 90°$). The purpose of these tests was to define a final HIRM geometry and to develop baseline data on lift, drag, and control effectiveness especially with regard to trim angles of attack. These baseline data were then used to define the test matrix for the definitive HIRM geometry. Data were taken at 2° increments in angle of attack for $0° < \alpha < 40°$ and at 5° increments for $40° < \alpha < 90°$. Based on these tests, a final geometry for HIRM was defined and a 0.44-scale model was built. Before the full-scale free flight tests, this model underwent static and oscillatory tests in the RAE (Bedford) 13- by 9-Foot Tunnel and rotary tests in the BAe (Warton) 18-Foot Tunnel. After the first series of free flights at DFRF, a 0.22-scale model was tested on the new rotary rig at the RAE (Bedford) 13- by 9-Foot Tunnel. Tunnel wind speed was 70 m/sec allowing for $N_{Re} = 1.5 \times 10^6$ (based on $\bar{c}$) which is close to the full-scale model flying at 40 m/sec at an altitude between 14 000 and 2000 ft (with $N_{Re} = 1.7 \times 10^6$ to 2.3×10^6). Additional rolling- and yawing-moment coefficients were measured for the full-scale free flight model in the RAE (Farnborough) 16.5-Foot Tunnel. A summary of available derivatives, their sources, and the figure in which each is used is given in table I.

Analysis Methods

A general flow chart for system identification analysis is given in figure 6.

First, an experiment is designed using all available a priori knowledge of the physical system to be identified. This knowledge includes results from previous experiments. Once the experiment has been performed and data have been gathered, the data are run through a compatibility check. The purpose of the compatibility check is to determine whether all data channels are self and cross consistent. The check should also allow for the estimation of bias or scale

factor errors in the data so as the make the measured data correctable.

After the data are brought into the most consistent shape possible, the analysis continues with model structure determination and parameter estimation. Here, a priori knowledge of the physical system and model building software such as stepwise regression are used to determine a set of models that are qualitatively adequate to explain the behavior of the system as recorded in the measured data. The model is completed by estimating any constants (parameters) associated with the determined model structure. This model is then verified by assessing its prediction capability using a data set that was not employed in the identification. If the verification is good, the process is complete, with the model being that which was verified. If the verification result is lacking, then the analyst must backtrack either to the experiment design stage or simply to the model structure determination stage. The return to the latter stage can pass through a data restructuring stage (such as data partitioning) in which the measured data are separated or combined in innovative ways to allow for better model structure determination. This inner loop continues until a successful verification is achieved or until all experiments and data restructuring have been exhausted.

The following paragraphs will focus on a data compatibility check; a model structure determination and parameter estimation; and, as was necessary for the analysis of these data, partitioning.

Data Compatibility

Each flight from the 1983 and 1986 series was first subjected to a test for data self-consistency (data compatibility). This check is performed by integrating the aircraft kinematic equations using measured values of angular rates and linear accelerations as inputs that are integrated to compute output variables consisting of Euler angles, total airspeed, angle of attack, and angle of sideslip. An algorithm reported in reference 8 was used. In addition to the simple integration, the algorithm allows the option of estimating values for bias and scale-factor errors on the input and output data that would minimize the sum of squares of differences between measured and computed values (residuals). Along with identifying bias and scale-factor corrections, the data compatibility check allows for an assessment of gross data problems such as sign reversals. If several sections of a flight yield consistent estimates of bias or scale factors, the data from that flight are corrected by applying that bias or scale-factor correction to the data prior to analysis. After these data were corrected, the analysis proceeded with the determination of model structure and the estimation of corresponding stability and control derivatives.

Data Restructuring

The general form of the aircraft equations of motion and aerodynamic model equations is found in the appendix. Nonlinear dependence of the aerodynamic force or moment coefficients on one or more variables leads to difficulty in postulation of a proper model structure, whereas lack of good information or lack of harmonic content in a maneuver leads to identifiability problems with some parameters. The large amplitude motions that often characterize drop model flight data can pose both of these problems. Multiple nonlinear dependence causes the entry of nonlinear terms in more than one variable when the modified stepwise regression (explained below) is applied to data from a maneuver. The variation of any potential independent variable (such as α, β, etc.) in a maneuver can be reduced for the purpose of analysis by dividing the maneuver into several subsets (with each subset covering a fraction of the total maneuver range) and then analyzing each subset independently. This process is called partitioning.

To understand the basis for partitioning, let

$$y(t) = f\left[x_1(t),\ x_2(t),\ \ldots,\ x_n(t)\right] \tag{1}$$

where x_i to x_n are the regressors formed from the airplane response and control variables. Now suppose that for any time t we want to eliminate the dependence of $y(t)$ on one of the $x_i(t)$, say $x_p(t)$. Then, by partitioning we mean redefining $y(t)$ on proper subsets of $\{x_1,\ x_2,\ \ldots,\ x_n\}$ as

$$y(\bar{x}_p, t) = \begin{cases} f_1\left[x_1(t),\ x_2(t),\ \ldots,\ x_{p-1}(t),\ x_{p+1}(t),\ \ldots,\ x_n(t)\right] \\ \qquad\qquad (x_{p_0} < x_p < x_{p_1}) \\ f_2\left[x_1(t),\ x_2(t),\ \ldots,\ x_{p-1}(t),\ x_{p+1}(t),\ \ldots,\ x_n(t)\right] \\ \qquad\qquad (x_{p_1} < x_p < x_{p_2}) \\ \qquad\qquad \vdots \\ f_m\left[x_1(t),\ x_2(t),\ \ldots,\ x_{p-1}(t),\ x_{p+1}(t),\ \ldots,\ x_n(t)\right] \\ \qquad\qquad (x_{p_{m-1}} < x_p < x_{p_m}) \end{cases} \tag{2}$$

where

$$\bar{x}_p = \frac{x_{p_{i+1}} + x_{p_i}}{2} \qquad (i = 1, 2, \ldots, m)$$

That is, each $(n+1)$-tuple in (x_i, y) is reduced to several n-tuples—each associated with a particular value on a small range of x_p. The supposition is that as the range defined by $x_{p_{i+1}} - x_{p_i}$ becomes

smaller, the variation in f due to x_p becomes less significant and reaches a level where it can be neglected. For example, an aircraft might perform a mostly lateral maneuver but with angle of attack α varying between 20° and 30°. Because of separation effects on the lifting surfaces in this α region, we could expect that the lateral aerodynamic force and moment coefficients C_Y, C_l, and C_n might well depend on α in a nonlinear way, i.e.,

$$C_n = C_n(\alpha, \beta, p, r, \delta_{\text{control}}) \tag{3}$$

Then, to partition, one would simply analyze the data in separate groupings as follows:

$$\left.\begin{aligned} (C_n)_{\bar{\alpha}=21°} &= C_n(\beta, p, r, \delta_{\text{control}}) \quad (20° < \alpha < 22°) \\ (C_n)_{\bar{\alpha}=23°} &= C_n(\beta, p, r, \delta_{\text{control}}) \quad (22° < \alpha < 24°) \\ &\vdots \\ (C_n)_{\bar{\alpha}=29°} &= C_n(\beta, p, r, \delta_{\text{control}}) \quad (28° < \alpha < 30°) \end{aligned}\right\} \tag{4}$$

That is, all data corresponding to $20° < \alpha < 22°$ are put into one group for analysis, data corresponding to parts of the maneuver in which $22° < \alpha < 24°$ are put into a second group, and so forth, until all data have been accounted for.

If any grouping still appears to be dependent on α, it can be subdivided further (assuming that a sufficient number of data points exist). In this example one can now analyze $C_n = f(\beta, p, r, \delta_{\text{control}})$ at characteristic values of α given by the mean value of α for each grouping. To be more specific, consider an application of the above process to data with the angle-of-attack time history shown in figure 7. All data corresponding to angles of attack less than 20° are put in bin 1, data with $20° < \alpha < 22°$ are put in bin 2, and so forth, until all data with $\alpha > 30°$ are put in bin 7. Notice that this partitioning procedure will often lead to non-time-contiguous data being analyzed in the same bin (as with bin 2 for sections of data at a time approximately equal to 3, 5, 19, 22, and 25 sec).

After the bins or subsets are established, the model structure determination and parameter estimation can proceed. The model structure determination is still necessary since large variations also may have occurred in variables other than the one on which the partitioning is based (for example, large variations in β while partitioning is with respect to α). The model structure determination and parameter estimation then proceed by applying a modified stepwise regression (MSR) algorithm to each bin or subset of partitioned data (ref. 9).

After partitioning for some individual maneuvers, the information content of the data to be analyzed may be inadequate. Indicators of this problem are a lack of identifiability for some parameters (because of large scatter or large standard error of parameter estimates) or cross plots of variables that indicate a lack of excitation in one or more variables. An example of cross plots of roll rate and sideslip angle (p versus β) for eight bins after partitioning one of the 1986 flights is given in figure 8. Figure 8(a) shows data that are minimally adequate in distribution and range for identification. Figures 8(d) and 8(e) are entirely adequate in both range and distribution within that range. Figure 8(h) is adequate in distribution pattern but is limited in range for both β and p. To increase the information content of the data being analyzed, several maneuvers can be combined and the combined set be partitioned; or, equivalently, the partitioned sets from equivalent α bins from several flights can be combined for model structure determination and parameter estimation using modified stepwise regression.

Model Structure Determination and Parameter Estimation

All the data from each bin are analyzed using a modified stepwise regression (MSR). As a modified version of the linear regression, this method can determine the structure of an aerodynamic model and estimate the model parameters. The determination of an adequate model (a model that fits the data and has good prediction capabilities) for the aerodynamic coefficients includes three steps: the postulation of terms that might enter the model, the selection of a model, and the verification of the model selected. The general form of aerodynamic model equations can be written as

$$y(t) = \boldsymbol{\theta}_0 + \boldsymbol{\theta}_1\, x_1(t) \ldots + \boldsymbol{\theta}_n\, x_n(t) \tag{5}$$

where $y(t)$ represents the resultant coefficient of aerodynamic force or moment. In the polynomial representation of the aerodynamic coefficient, $\boldsymbol{\theta}_1$ to $\boldsymbol{\theta}_n$ are the stability and control derivatives. (The linear stability and control derivatives are of the form $C_{A_{x_i}} \approx \partial C_A/\partial x_i$ where $A = X, Y, Z, l, m,$ or n and $x_i = \alpha, \beta, p, r,$ or δ_{control}; nonlinear derivatives are of the form $\partial^{n_1} C_A/\partial x_i^{i_1} \ldots \partial x_k^{k_1}$ where $n_1 = 2, 3, \ldots, n; i, \ldots, k = 1, 2, \ldots, n; i_1, \ldots, k_1 = 1, 2, 3, 4, 5;$ and $n_1 = i_1 + \ldots + k_1$. For example, in $\partial^2 C_l/\partial\alpha\partial\beta, C_A = C_l, n_1 = 2; x_1 = \alpha, x_2 = \beta;$ and $i_1 = 1, i_2 = 1$. The symbol $\boldsymbol{\theta}_0$ is the value of any particular coefficient corresponding to the reference flight conditions, and x_i to x_n are the regressors

formed from the airplane output and control variables and their combinations.

Postulating the aerodynamic model equations by selecting the candidate regressors is followed by the determination of significant terms among the candidate variables and the estimation of the corresponding parameters. The variable chosen for entry into the regression equation is the one that has the largest correlation with y after adjusting for the effect on y of the variables already selected. The parameters are estimated by minimizing the cost function

$$J_{\mathrm{SR}} = \sum_{i=1}^{N} \left[y(i) - \hat{\theta}_0 - \sum_{j=1}^{\ell} \hat{\theta}_j \, x_j(i) \right]^2 \qquad (6)$$

where N is the number of data points and $\ell+1$ is the number of parameters in the regression equation.

At every step of the regression, the variables incorporated into the model in previous stages and a new variable entering the model are reexamined. Any variable that provides a nonsignificant contribution as given by its F-statistic (due to correlation with more recently added terms) is removed from the model by the algorithm. The process of selecting and checking variables continues until no more variables are admitted to the equation and no more are rejected. Experience shows, however, that the model based only on the significance of individual parameters in the model in equation (6) can still include too many terms and therefore may have poor prediction capabilities. Therefore, three quantities are examined for each model structure as criteria for an adequate model, and they are presented as follows:

1. The computed value of the F-statistic. This is given as the ratio of regression mean square to residual mean square and is calculated as

$$F = \frac{\left(\hat{\boldsymbol{\Theta}}^T \mathbf{X}^T \mathbf{Y} - N\bar{y}\right)^2}{(n-1)s^2} \qquad (7)$$

where

$$\bar{y} = \frac{1}{N} \sum_{i=1}^{N} y(i)$$

$$s^2 = \frac{1}{N-n} \sum_{i=1}^{N} \left[y(i) - \hat{y}(i)^2 \right]$$

and the superscript T denotes a transpose matrix. Equation (7) was developed for the model given by equation (1) and can be expressed in matrix notation as

$$\mathbf{Y} = \mathbf{X}\boldsymbol{\Theta} + \boldsymbol{\varepsilon} \qquad (8)$$

The F-value can be associated with an estimate of the standardized total mean-square error of estimation for the data $\mathbf{X}$ as shown in reference 10. The model with a maximum F-value has already been recommended in reference 11 as the "best" one for a given set of data.

2. The value of the square of the multiple-correlation coefficient (R^2). This indicates the proportion of the variation due to terms other than $\boldsymbol{\theta}_0$ in the model. The value of R^2 is obtained from the equation

$$R^2 = \frac{\hat{\boldsymbol{\Theta}}^T \mathbf{X}^T \mathbf{Y} - N\bar{y}^2}{\mathbf{Y}^T \mathbf{Y} - N\bar{y}^2} \qquad (9)$$

3. The residuals $\hat{\boldsymbol{\varepsilon}}(i)$. For an adequate model, the sequence of the residuals $\hat{\boldsymbol{\varepsilon}}(i)$ should be close to a random sequence that is uncorrelated and Gaussian.

The use of these three criteria is demonstrated in references 12 and 13.

Results

Data Compatibility

Data received from the United Kingdom exhibited good compatibility for both the 1983 and 1986 flight series. Because of the large excitation just after release from the helicopter, due to the mismatch of tow airspeed and angle of attack with those for free flight, the beginning of each flight offered the best opportunity for a compatibility check. An example of the highly excited beginning of one of the 1986 flights is given in figure 9. Figure 9(a) gives the measured and computed time histories for output variables V, α, θ, β, and ϕ. Figure 9(b) gives the residual time histories (the difference between the measured and computed values for the corresponding output variable in fig. 9(a)) for V, α, θ, β, and ϕ. Figure 9(c) gives the time histories of the linear accelerations and angular rates that are the inputs to the data compatibility algorithm. The computed values in figure 9 are for the case in which biases were estimated and removed from a_x, a_y, a_z, p, q, and r. The estimated bias values for a_x, a_y, a_z, p, q, and r for this part of the flight were $0.018g, -0.015g, -0.089g, 0.02$ rad/sec, -0.002 rad/sec, and 0.03 rad/sec, respectively. These bias values are small relative to the ranges of the analyzed maneuver. Moreover, when several different flights or different sections of data from one flight were analyzed, no consistent bias values could be found. Therefore, it was determined that no bias

corrections would be made before analysis. The effect of this decision on the accuracy of estimated stability and control derivatives is thought to be small (heuristically) but cannot actually be determined.

Aerodynamic Model Structure

Lateral. Model structures were determined by applying MSR to sections of data identified as "individual maneuvers" and to bins of data created by partitioning. The individual maneuvers were chosen to be portions of a flight in which there were significant control surface movements ($\pm 2°$ or $3°$) and significant vehicle response to those movements (signal to noise greater than 1 visually on plotted time histories). An adequate width of bins for the partitioned data was determined, in part, by the results of several MSR applications described as follows: First, a nominal bin width of $2°$ angle of attack was chosen. This $2°$ width often precipitated the inclusion of nonlinear terms that indicated angle-of-attack dependence (such as $p\alpha, p\alpha^2, \beta\alpha$, and so forth). Then, the bin width was reduced and MSR was applied again. This process continued until the terms indicating a variation with angle of attack were no longer significant to MSR. In areas of highly nonlinear aerodynamics, this bin width was $0.5°$; in the more benign α ranges, a bin width of $1.0°$ was adequate. Because of the amount of maneuvering in the range of α from $24°$ to $28°$ during each flight, there were always enough data to make such small bins amenable to analysis.

With the bin widths small enough to preclude terms indicative of the variation of a parameter with angle of attack, nonlinearities in other variables such as sideslip or roll rate should become visible (ref. 13). An example of such a nonlinearity is demonstrated in figure 10 where the effect of the entry of β^3 into the equation for the rolling-moment coefficient is shown. The variable β^3 was a consistent entry for the two unaugmented flights HD8 and HD19 in the bins for $24° < \alpha < 26°$. For these bins, $-4° < \beta < 9°$. A similar variation was found in data from the RAE (Farnborough) 16.5-Foot Tunnel as plotted in figure 10 for the purpose of comparison. Although the effect is small for $-5° < \beta < 5°$, it means a reduction in the rolling-moment coefficient by almost 70 percent for $\beta \approx 8°$ and a change in sign for the dihedral effect C_{l_β} from negative to positive at $\beta \approx 5°$. Since the flight was asymmetric, no data were available for $\beta < -4°$.

Although the wind-tunnel tests indicated a $(pb/2V)^3$ dependence for C_l (ref. 6), only two bins from the unaugmented flights and no bins from the augmented flights required nonlinear terms in $pb/2V$. It is postulated that nonlinear roll rate effects were not seen in the flight data because most in-flight nondimensional roll rates were less than 0.04, the value at which the wind-tunnel nonlinearities became apparent. The remainder of the model structure was linear in β, p, r, δ_d, and δ_r when these variables were significantly excited. In particular, models derived from partitioned data from the 1986 series consistently contained β and δ_d in the side-force equation, β, p, and δ_d in the rolling-moment equation, and β and δ_d in the yawing-moment equation. Several terms that are normally identifiable in system identification applications (particularly δ_r for the side-force coefficient and r and δ_r for the yawing-moment coefficient) were not identifiable from the data analyzed.

Longitudinal. Both the individual maneuvers and the partitioned data were analyzed for model structure using MSR. Several of the 1983 flights indicated pitching-moment-coefficient dependence on roll rate p and sideslip through β^2. Two of the individual maneuvers in the 1986 flights required an α^2 term to achieve an adequate model for the vertical-force coefficient. None of the partitioned data gave rise to nonlinear α dependence since the bin widths were chosen specifically to eliminate such dependence. In addition, $C_{m_{\delta h}}$ was not identifiable (did not provide a statistically significant improvement in fit) in several of the 1983 individual maneuvers. This lack of identifiability is unusual for $C_{m_{\delta h}}$ and no reason was found for it.

Derivative Values

All derivative comparisons were made using the adequate model structure as determined by MSR. This means that the β^3 term with $C_{l_{\beta^3}}$ is in the rolling-moment equation. The effect of adding the β^3 term is to make the linear derivative C_{l_β} of the nonlinear model slightly more negative when compared with the linear model.

Lateral. The sideslip derivatives are given in figure 11 for both the 1983 and 1986 flights. The flight-estimated values are compared with published wind-tunnel results. The change in side-force coefficient due to change in sideslip C_{Y_β} is considerably less when estimated from flight tests than when estimated from wind-tunnel tests. This result is seen consistently in the 1983 series for both canard settings and in the 1986 series for $\delta_c = 0°$.

The derivative C_{l_β} from the 1983 series does not reflect the canard effect seen in the wind tunnel. The flight results for $\delta_c = -10°$ show approximately 60 percent of the dihedral effect that was measured in

the wind tunnel for $18° < \alpha < 26°$. The flight value stays negative at $\alpha = 30°$ and the wind-tunnel value goes to zero. The flight-derived values for $\delta_c = 0°$ also generally indicate reduced dihedral effect when compared with the wind-tunnel measurements. The 1986 tests tend to confirm the 1983 results for $\delta_c = 0°$ except for two values from the unaugmented flight HD8. No reason could be found for this discrepancy except to note that HD8 was the 1986 flight with the largest β excitation and in which $C_{l_{\beta^3}}$ became identifiable. The 1983 series yields C_{n_β} values that follow the wind-tunnel trends. However, the 1983 data for $\delta_c = -10°$ indicate $C_{n_\beta} < 0$ by $\alpha = 19°$, whereas the wind tunnel indicates $C_{n_\beta} = 0$ at $\alpha = 20.5°$. The 1983 data for $\delta_c = 0°$ indicate C_{n_β} to be more negative than that indicated by the wind tunnel for $25° < \alpha < 30°$. This latter statement is confirmed by the 1986 data for $24° < \alpha < 28°$. Combining directional stability C_{n_β} with the dihedral effect C_{l_β} through the effect of the inertia ratio I_Z/I_X gives the parameter

$$C_{n_{\beta,\mathrm{dyn}}} = C_{n_\beta} - \frac{I_Z}{I_X} C_{l_\beta} \sin\alpha$$

In highly dynamic maneuvers, the sign of $C_{n_{\beta,\mathrm{dyn}}}$ indicates stability better than simple C_{n_β}. The $C_{n_{\beta,\mathrm{dyn}}}$ for the flight analysis was calculated using C_{n_β} values from the flight data analysis shown in figure 11 and approximating C_{l_β} values from the local slopes of the C_l versus β nonlinear model curve in figure 10. Figure 12 shows that for the 1986 results, the β^3 terms in the rolling-moment coefficient give $C_{n_{\beta,\mathrm{dyn}}} > 0$ for $0° < \beta < 5°$ and $\alpha \approx 25°$, but its value rapidly decreases to a value of -0.64 for $\beta = \pm 7°$. Reference 3 indicates that $C_{n_{\beta,\mathrm{dyn}}} > 0$ for $\alpha < 30°$.

Of the three yaw rate derivatives, only the cross derivative C_{l_r} was consistently identifiable and still showed wide scatter (fig. 13). For the $\delta_c = -10°$ case in the 1983 flights, the flight estimates agree well with the wind-tunnel values. However, for $\delta_c = 0°$ in 1983, the C_{l_r} flight estimates generally exceed the wind-tunnel values for $24° < \alpha < 28°$. The 1986 estimates ($\delta_c = 0°$ and $-5°$) appear to confirm the 1983 flight results ($\delta_c = 0°$). The sparse flight estimates for C_{Y_r} and C_{n_r} are presented for completeness. The yaw rate and yawing moment were not well-excited in the 1986 flights because there were no rudder inputs designed and executed for directional excitation. Moreover, for the augmented flights (HAD9 and HAD16), control inputs were actually used to suppress lateral-directional excitation.

The roll rate derivatives are given in figure 14. Both rotary and oscillatory wind-tunnel measurements are presented for comparison. These tunnel measurements are for $\delta_c = -10°$ in all figures. The discrepancy between sets of values from the oscillatory and rotary tests has already been noted in reference 6. The flight-derived values indicate a loss of roll damping for $21° < \alpha < 25°$ for $\delta_c = -10°$, whereas the rotary data indicate such a loss only for $23° < \alpha < 25°$. The oscillatory data indicate no loss of damping in this region. The 1983 data for $\delta_c = 0°$ show damping to be maintained for $22° < \alpha < 28°$, whereas the 1986 data indicate about one-half the level seen in the 1983 data for $\delta_c = 0°$. That difference could be due to the smaller excitation of roll rate in the 1986 series combined with the nonlinearities in $pb/2V$ at higher roll rates. The C_{n_p} values were not identifiable for the 1986 series.

The control effectiveness of a differential horizontal tail was usually identifiable for all three coefficients C_Y, C_l, and C_n. The results are given in figure 15. Only $C_{Y_{\delta d}}$ from the 1986 series shows any consistent difference from the wind-tunnel values. The limited number of points plotted for the 1986 flights stems from the fact that lateral controls were used only on the augmented flights (HAD9 and HAD16) and then only in a 5-sec open-loop sequence to eliminate excessive bank angle. Therefore, there was simply not enough data outside the main area of interest in angle of attack.

Longitudinal. The two primary stability derivatives C_{L_α} and C_{m_α} are given in figure 16. All flights, except HAD16, were flown with the c.g. location at 12.5-percent $\bar{c}$. All wind-tunnel values are referenced to that location. Flight HAD16 was flown with the c.g. aft at 22.5-percent $\bar{c}$. This led to approximately 10° less horizontal stabilator for trim in the angle-of-attack range from 16° to 40°. A cluster of C_{L_α} data points is shown scattered around the wind-tunnel values, and the trends seen in the wind tunnel near $\alpha = 22°$ are not apparent from flight. The effect of the c.g. position is not apparent in figure 16(b) since there are too few data points to verify wind-tunnel results. Values for the damping-in-pitch derivative C_{m_q} are plotted in figure 17. Pitch rate was well-excited in the 1983 series because of cross coupling with the large lateral motion. Hence, several individual maneuvers and bins provided estimates of C_{m_q} (fig. 17(b)). However, for the 1986 series, as mentioned earlier, the SAS prevented excessive longitudinal response and the lateral oscillations were not as severe as in the 1983 series. Thus, only four maneuvers out of the entire 1986 series produced an identifiable C_{m_q}, and these values are plotted in figure 17(a).

The horizontal tail effectiveness $C_{m_{\delta h}}$ is plotted in figure 18. This derivative was consistently identifiable from the positioned data in both the 1983 and 1986 series. The average flight value indicates that the effectiveness of the horizontal stabilator is degraded in flight to about 65 percent of its wind-tunnel value.

Eigenstructure Analysis of Lateral Modes

The wind-tunnel-determined roll, Dutch roll, lateral phugoid, and spiral modes were discussed in reference 4 to give a better physical overview of the expected HIRM flight characteristics. Figure 24 in that report is repeated here as figure 19. Figure 20 presents damping and frequency as given by the average of the flight-derived derivative estimates for each angle of attack. Also, flight air density, inertias, and mass were used to derive the values in figure 20. Significant differences between figures 19 and 20 include a change in notation (k_R, k_S, and k_D become k_1, k_2, and k_3, respectively) and a change in scale for the middle graph (k_D to k_3). The change in notation eliminates reference to roll, Dutch roll, and spiral modes for the flight-derived values, although the eigenvalues from flight-derived derivatives appear to separate out these usual lateral modes. A study of the eigenvectors (fig. 21) indicates that a different set of three modes is present. Figure 21 gives plots of eigenvectors corresponding to each flight-derived eigenvalue at intervals of 2° in angle of attack. The first column indicates a large bank-angle component (ϕ) accompanying the heading component (Ψ). The eigenvalue that would normally represent roll damping is associated with the eigenvector plotted in the second column. Even though bank angle (ϕ) mostly dominates, a small sideslip component (β) is present and grows steadily until $\alpha = 28°$ where it is then equal to ϕ. Finally, the third column of vectors shows that the undamped oscillatory mode is basically a roll-dominated (bank angle) mode; it only begins to resemble a true Dutch roll at $\alpha = 30°$.

Verification

The final stage of identification, as seen in figure 6, is model verification. One phase of verification has already been completed by making sure that the derivative estimates are physically reasonable and comparing them with wind-tunnel test results. The other verification technique checks the prediction capability of the model by integrating the aircraft equations of motion for one of the flight maneuvers. A batch simulation was used with the math model determined by fairing a line through and averaging the flight results given in this report. A three-degree-of-freedom simulation was used with the longitudinal response variables taken as measured. Figure 22 shows the results of that simulation and the angle-of-attack time history using a maneuver from HD1. The frequencies predicted by the model are good and the amplitudes of the oscillations exceed those recorded in flight. An additional point of view was gained by comparing the predicted and measured time histories for lateral force and moment coefficients as shown in figure 23.

Conclusions

Flight data from two series of flights of the Royal Aerospace Establishment (RAE) high-incidence research model (HIRM) have been analyzed. Model structure and the corresponding stability and control derivatives were determined. These results were compared with available wind-tunnel results, and the following conclusions are presented:

1. Partitioning and modified stepwise regression can provide stability and control derivatives from data where individual maneuvers were not intended or were not suitable for system identification.
2. Nonlinearities in a variable can be eliminated by partitioning, thus allowing for nonlinearities in other variables to be visible.
3. Data from a control-surface-initated response at several flight conditions are more useful than data from self-excited oscillations because data on and beyond the roll rate and sideslip boundaries of the self-excited motion can be analyzed, thus giving more information on those boundaries.
4. Estimated parameters from the 1986 flights confirmed, in general, the results from the 1983 flights with a symmetric canard deflection of 0° except for the values of damping-in-roll derivatives.
5. The vehicle exhibits three unusual roll-dominated lateral modes near an angle of attack of 24°.
6. The linear model on the lateral variables was adequate for each bin except those few where cubic sideslip dependence (β^3) was entered into the rolling-moment coefficient yielding a corresponding nonlinear derivative ($C_{l_{\beta^3}}$).

NASA Langley Research Center
Hampton, VA 23665-5225
August 21, 1989

Appendix

Airplane Equations of Motion and Postulated Models

The airplane equations of motion are referred to the body axes. They are based on the assumption that the airplane is a rigid body. The equations have the form

$$\dot{u} = -qw + rv - g\sin\theta + \frac{\rho V^2 S}{2m} C_X$$

$$\dot{v} = -ru + pw + g\cos\theta\sin\phi + \frac{\rho V^2 S}{2m} C_Y$$

$$\dot{w} = -pv + qu + g\cos\theta\cos\phi + \frac{\rho V^2 S}{2m} C_Z$$

$$\dot{p} = \frac{I_Y - I_Z}{I_X} qr + \frac{I_{XZ}}{I_X}(pq + \dot{r}) + \frac{\rho V^2 Sb}{2I_X} C_l$$

$$\dot{q} = \frac{I_Z - I_X}{I_Y} pr + \frac{I_{XZ}}{I_Y}(r^2 - p^2) + \frac{\rho V^2 S\bar{c}}{2I_Y} C_m$$

$$\dot{r} = \frac{I_X - I_Y}{I_Z} pq + \frac{I_{XZ}}{I_Z}(\dot{p} - qr) + \frac{\rho V^2 Sb}{2I_Z} C_n$$

$$\dot{\phi} = p + (q\sin\phi + r\cos\phi)\tan\theta$$

$$\dot{\theta} = q\cos\phi - r\sin\phi$$

For the stepwise regression method, the equations of motion can be formulated as

$$\frac{mg}{\bar{q}S} a_X = C_X$$

$$\frac{mg}{\bar{q}S} a_Y = C_Y$$

$$\frac{mg}{\bar{q}S} a_Z = C_Z$$

$$\frac{I_X}{\bar{q}Sb}\left[\dot{p} - \frac{I_Y - I_Z}{I_X} qr - \frac{I_{XZ}}{I_X}(pq + \dot{r})\right] = C_l$$

$$\frac{I_Y}{\bar{q}S\bar{c}}\left[\dot{q} - \frac{I_Z - I_X}{I_Y} pr - \frac{I_{XZ}}{I_Y}(r^2 - p^2)\right] = C_m$$

$$\frac{I_Z}{\bar{q}Sb}\left[\dot{r} - \frac{I_X - I_Y}{I_Z} pq - \frac{I_{XZ}}{I_Z}(\dot{p} - qr)\right] = C_n$$

For small-amplitude maneuvers, the aerodynamic coefficients are postulated as functions of the state and input variables and their combinations, and they are presented as follows:

1. The longitudinal coefficients C_X, C_Z, and C_m as functions of α, $q\bar{c}/2V$, δ_h, α^2, $(q\bar{c}/2V)\alpha$, $\delta_h\alpha$, β^2, $\alpha\beta^2$, α^3, α^4, α^5, α^6, α^7, and α^8.

2. The lateral coefficients C_Y, C_l, and C_n as functions of β, $pb/2V$, $rb/2V$, δ_d, δ_r, $\beta\alpha$, $(pb/2V)\alpha$, $(rb/2V)\alpha$, $\delta_d\alpha$, $\delta_r\alpha$, $\beta\alpha^2$, $(pb/2V)\alpha^2$, $(rb/2V)\alpha^2$, $\delta_d\alpha^2$, $\delta_r\alpha^2$, β^2, β^3, β^4, β^5, $(pb/2V)^2$, $(pb/2V)^3$, $\beta^3\alpha$, α, α^2, and α^3.

The variables in both model forms represent the increments with respect to their trim values. In the equation for the pitching-moment coefficient, the term $\dot{\alpha}$ was not explicitly included to avoid identifiability problems that occur because of the high correlation between $\dot{\alpha}$ and q. Relationships between parameters in the expressions for $C_m(\alpha, \beta, q, \delta_h)$ and for $C_m(\alpha, \dot{\alpha}, \beta, q, \delta_h)$ can be found in reference 13.

References

1. Moss, G. F.; Ross, A. Jean; and Butler, G. F.: *A Programme of Work on the Flight Dynamics of Departure Using a High Incidence Research Model (HIRM).* Tech. Memo Aero 1950, British Royal Aircraft Establ., July 1982.
2. Klein, V.; and Mayo, M. H.: Estimation of Aerodynamic Parameters From Flight Data of a High Incidence Research Model. *ICAS Proceedings, 1986—15th Congress of the International Council of the Aeronautical Sciences,* P. Santini and R. Staufenbiel, eds., c.1986, pp. 739–747. (Available as ICAS-86-5.5.2.)
3. Ross, A. Jean; and Reid, G. E. A.: The Development of Mathematical Models for a High Incidence Research Model. *Part 1: Analysis of Static Aerodynamic Data.* TR 83037, British Royal Aircraft Establ., Apr. 1983.
4. Ross, A. Jean; and Reid, G. E. A.: The Development of Mathematical Models for a High Incidence Research Model (HIRM). *Part 2: Analysis of Dynamic Test Data.* TR 84072, British Royal Aircraft Establ., July 1984.
5. Ross, A. Jean; and Edwards, Geraldine F.: Correlation of Predicted and Free-Flight Responses Near Departure Conditions of a High Incidence Research Model. *Unsteady Aerodynamics—Fundamentals and Applications to Aircraft Dynamics,* AGARD-CP-386, Nov. 1985, pp. 31-1–31-13.
6. O'Leary, C. O.; and Rowthorn, E. N.: New Rotary Rig at RAE and Experiments on HIRM. *Aeronaut. J.,* vol. 90, no. 900, Dec. 1986, pp. 399–409.
7. Ross, A. Jean; Edwards, Geraldine F.; Klein, Vladislav; and Batterson, James G.: Validation of Aerodynamic Parameters at High Angles of Attack for RAE High Incidence Research Models. *A Collection of Technical Papers—AIAA Atmospheric Flight Mechanics Conference,* Aug. 1987, pp. 296–304. (Available as AIAA-87-2558.)
8. Klein, Vladislav; and Morgan, Dan R.: *Estimation of Bias Errors in Measured Airplane Responses Using Maximum Likelihood Method.* NASA TM-89059, 1987.
9. Batterson, James G.; and Klein, Vladislav: Partitioning of Flight Data for Aerodynamic Modeling of Aircraft at High Angles of Attack. *A Collection of Technical Papers—AIAA Atmospheric Flight Mechanics Conference,* Aug. 1987, pp. 444–451. (Available as AIAA-87-2621.)
10. Hocking, R. R.: The Analysis and Selection of Variables in Linear Regression. *Biometrics,* vol. 32, no. 1, 1976, pp. 1–49.
11. Hall, W. Earl, Jr.; Gupta, Narenda K.; and Tyler, James S., Jr.: Model Structure Determination and Parameter Identification for Nonlinear Aerodynamic Flight Regimes. *Methods for Aircraft State and Parameter Identification,* AGARD-CP-172, May 1975, pp. 21-1–21-21.
12. Klein, Vladislav; and Batterson, James G.: *Determination of Airplane Model Structure From Flight Data Using Splines and Stepwise Regression.* NASA TP-2126, 1983.
13. Klein, Vladislav; Batterson, James G.; and Murphy, Patrick C.: *Determination of Airplane Model Structure From Flight Data by Using Modified Stepwise Regression.* NASA TP-1916, 1981.

Table I. Summary of Wind-Tunnel Tests and Figures Containing the Results

Derivative	Model size	Test	RAE tunnel	Reference	Figure
C_{L_α}	0.36	Static	No. 2 $11\frac{1}{2}$- by 8-Foot	3	16
C_{m_α}	0.36	Static	No. 2 $11\frac{1}{2}$- by 8-Foot	3	16
$C_{m_{\delta h}}$	.36	Static	No. 2 $11\frac{1}{2}$- by 8-Foot	3	18
C_{m_q}	.44	Oscillatory	13- by 9-Foot	4	17
C_{Y_β}	0.36	Static	No. 2 $11\frac{1}{2}$- by 8-Foot	3	11
$C_{Y_{\delta d}}$	.36	Static	No. 2 $11\frac{1}{2}$- by 8-Foot	3	15
C_{Y_r}	.44	Oscillatory	13- by 9-Foot	4	13
C_{l_β}	1.00	Static	16.5-Foot	5	10, 11
$C_{l_{\delta d}}$	.36	Static	No. 2 $11\frac{1}{2}$- by 8-Foot	3	15
C_{l_r}	.44	Oscillatory	↓	4	13
C_{l_p}	.44	Oscillatory	↓	6	14
$C_{l_{\dot{p}}}$	.22	Rotary	↓	6	14
C_{n_β}	1.00	Static	16.5-Foot	5	11
$C_{n_{\delta d}}$	.36	Static	No. 2 $11\frac{1}{2}$- by 8-Foot	3	15
C_{n_r}	.44	Oscillatory	No. 2 $11\frac{1}{2}$- by 8-Foot	4	13
C_{n_p}	.44	Oscillatory	13- by 9-Foot	6	14
$C_{n_{\dot{p}}}$	.22	Rotary	13- by 9-Foot	6	14

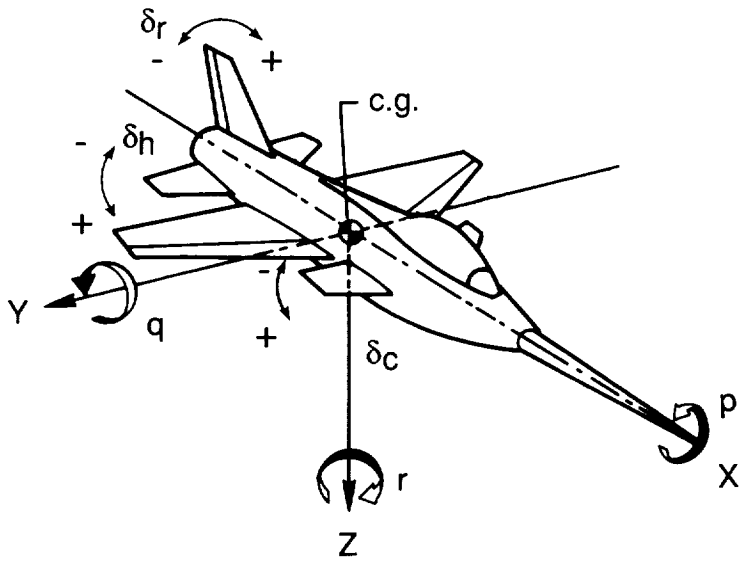

(a) Drawing indicating body system of axes, positive sense of angular rates, and sense of control surface deflections.

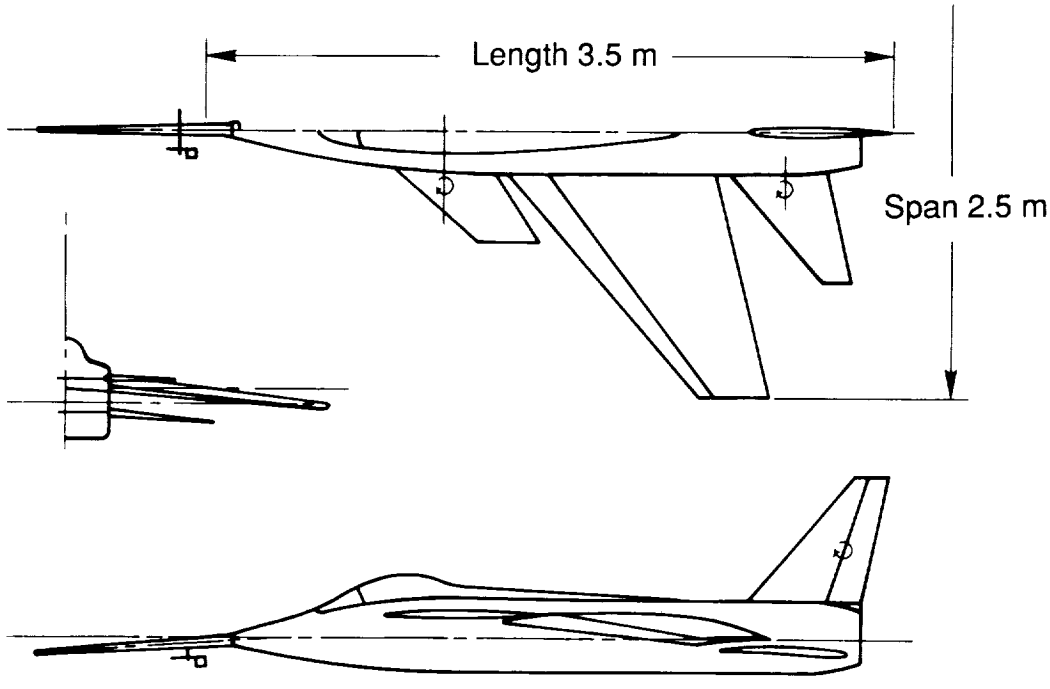

(b) Three-view drawing.

Figure 1. Drawings of the model.

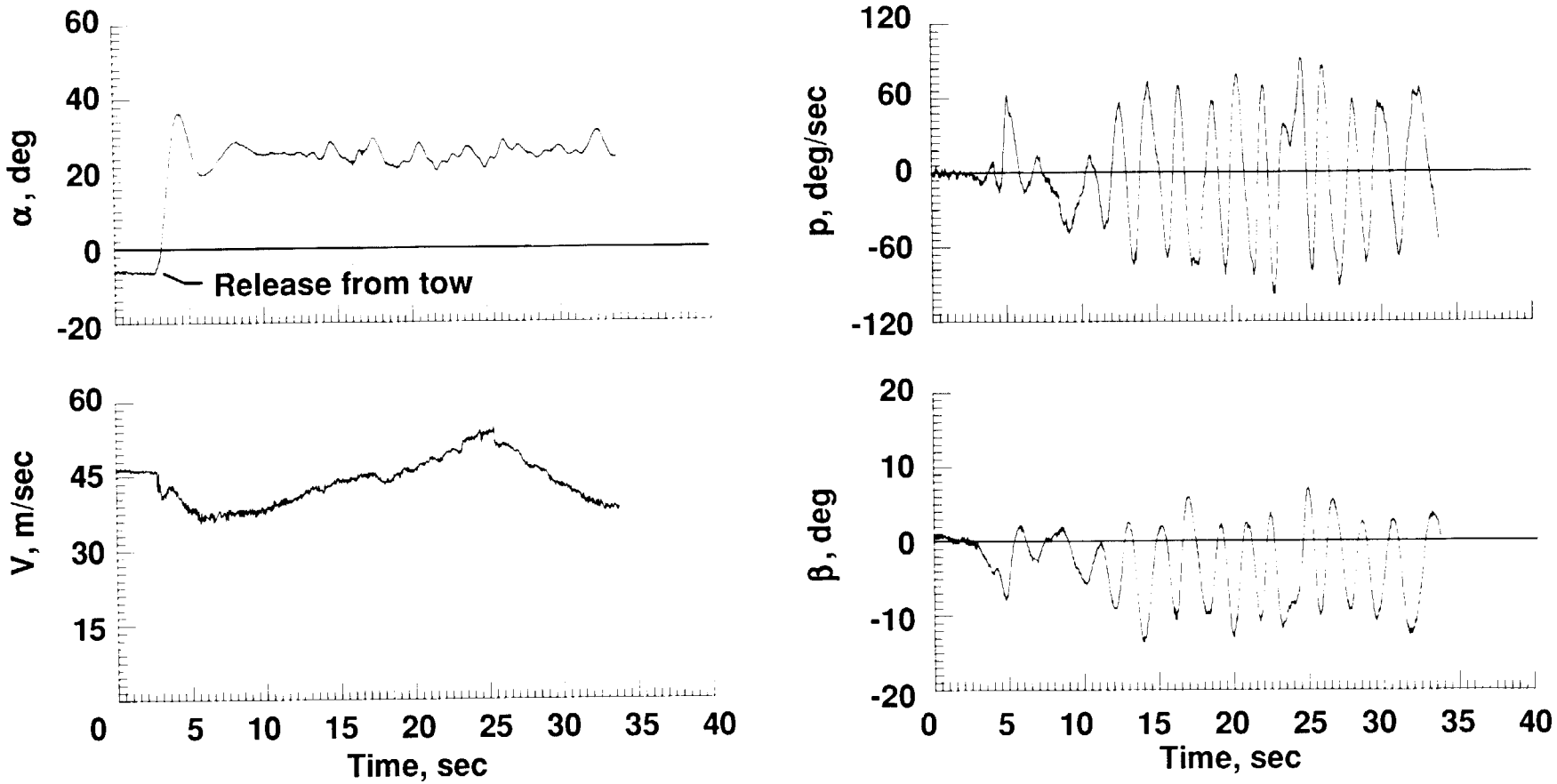

(a) α and V versus time.

(b) p and β versus time.

Figure 2. Time histories for selected input and response variables for the beginning of one of the unaugmented 1983 flights.

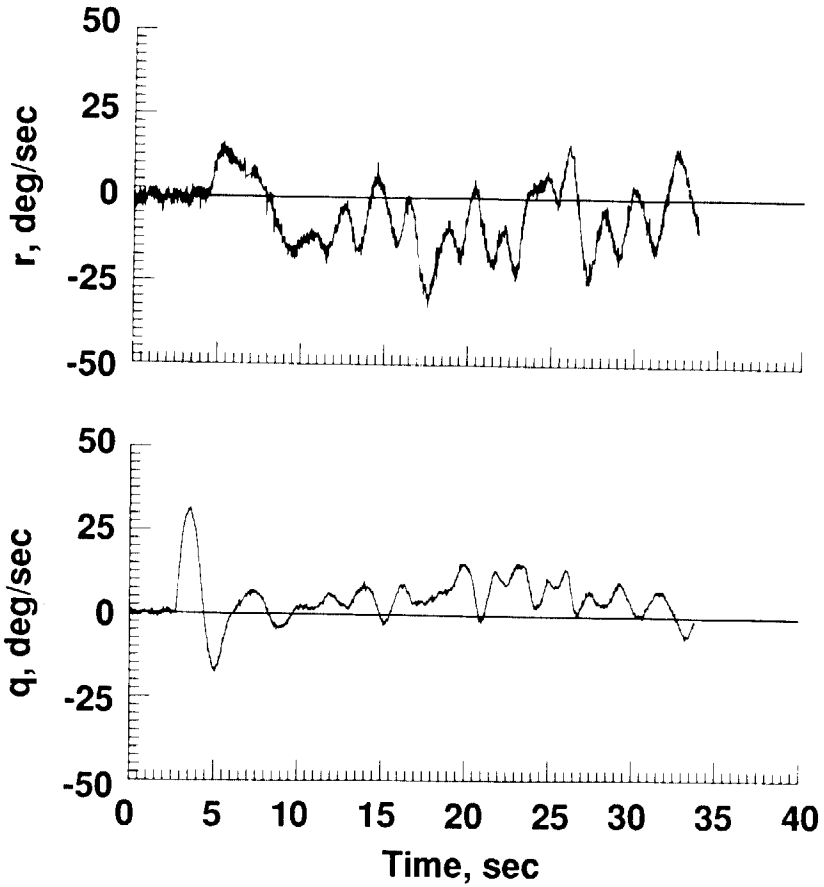

(c) r and q versus time.

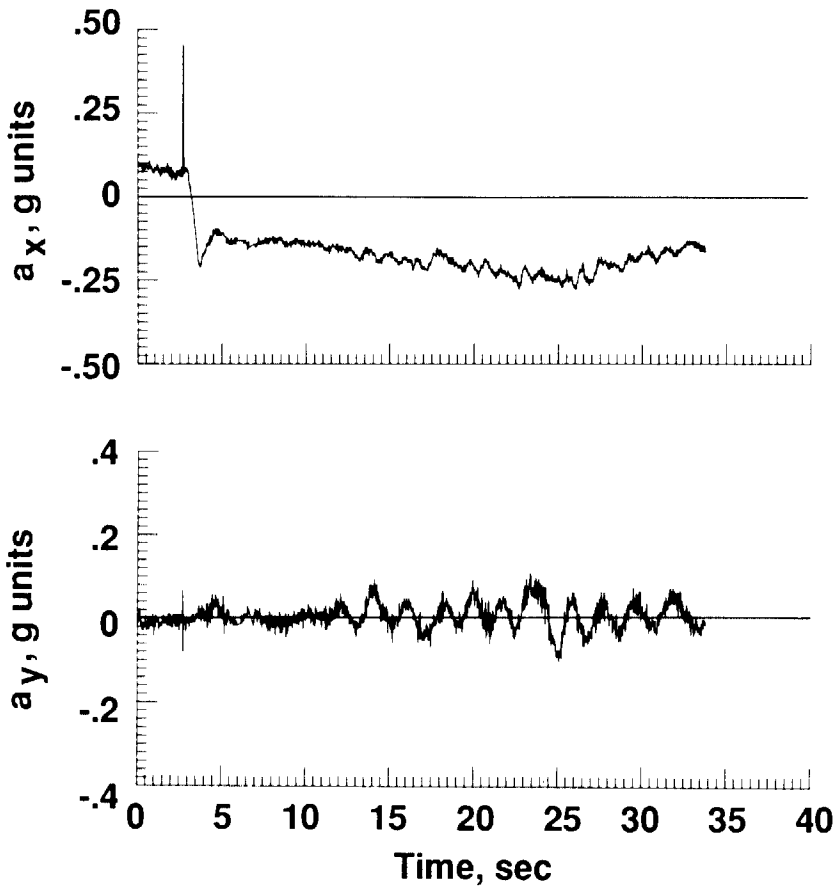

(d) a_x and a_y versus time.

Figure 2. Continued.

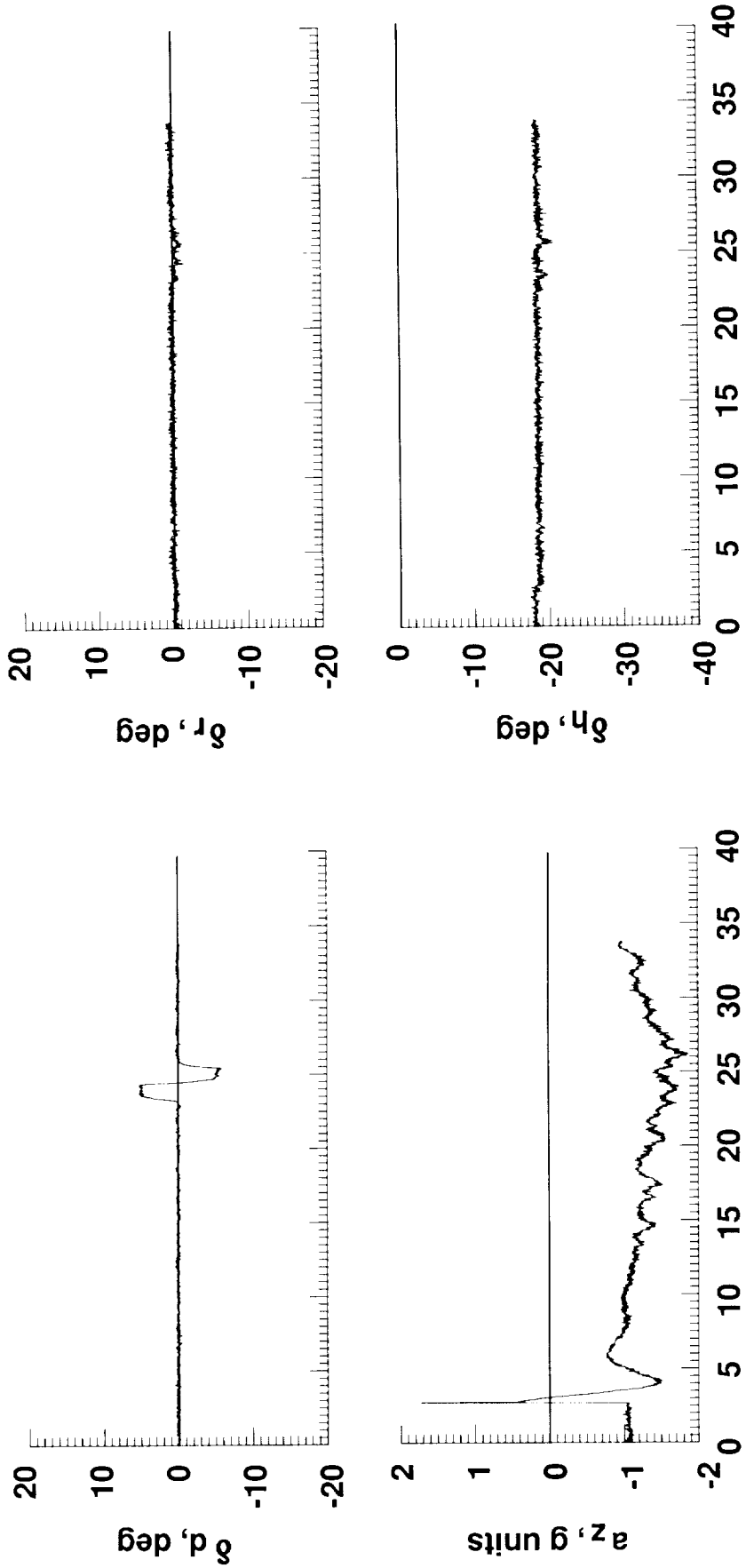

(e) δ_d and a_z versus time.

(f) δ_r and δ_h versus time.

Figure 2. Continued.

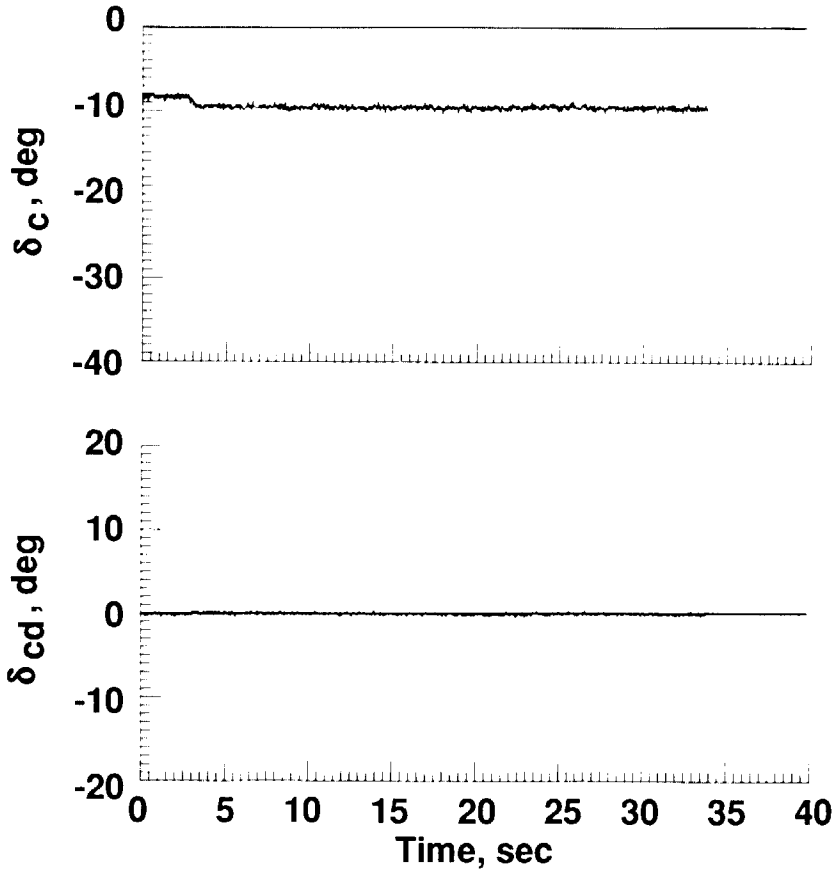

(g) δ_c and δ_{cd} versus time.

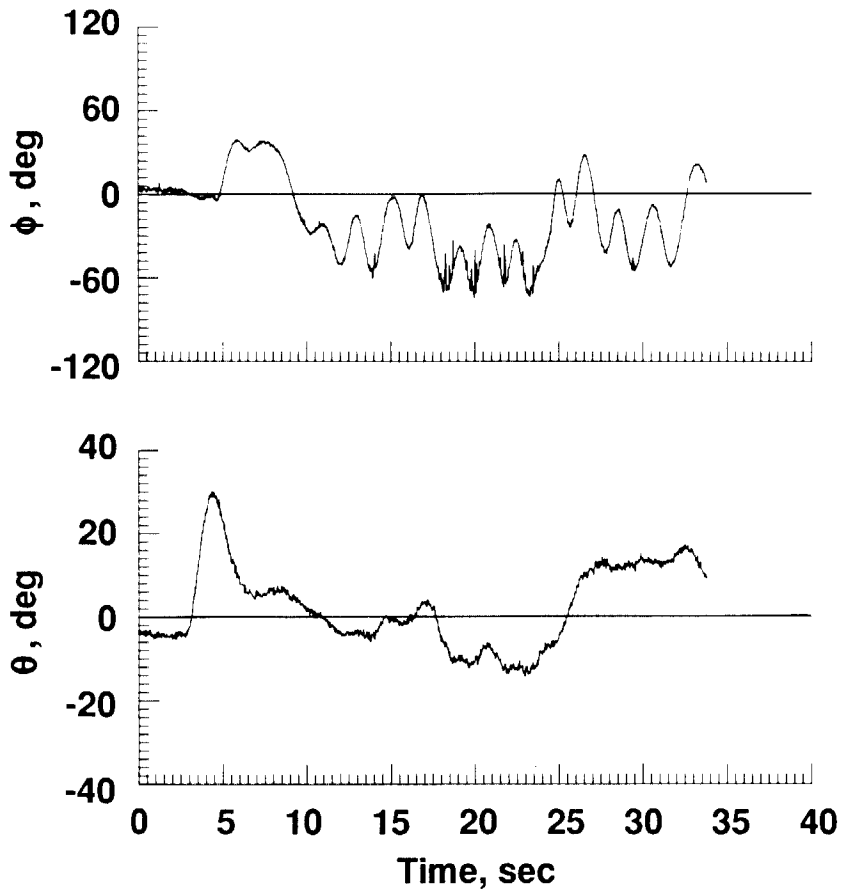

(h) ϕ and θ versus time.

Figure 2. Concluded.

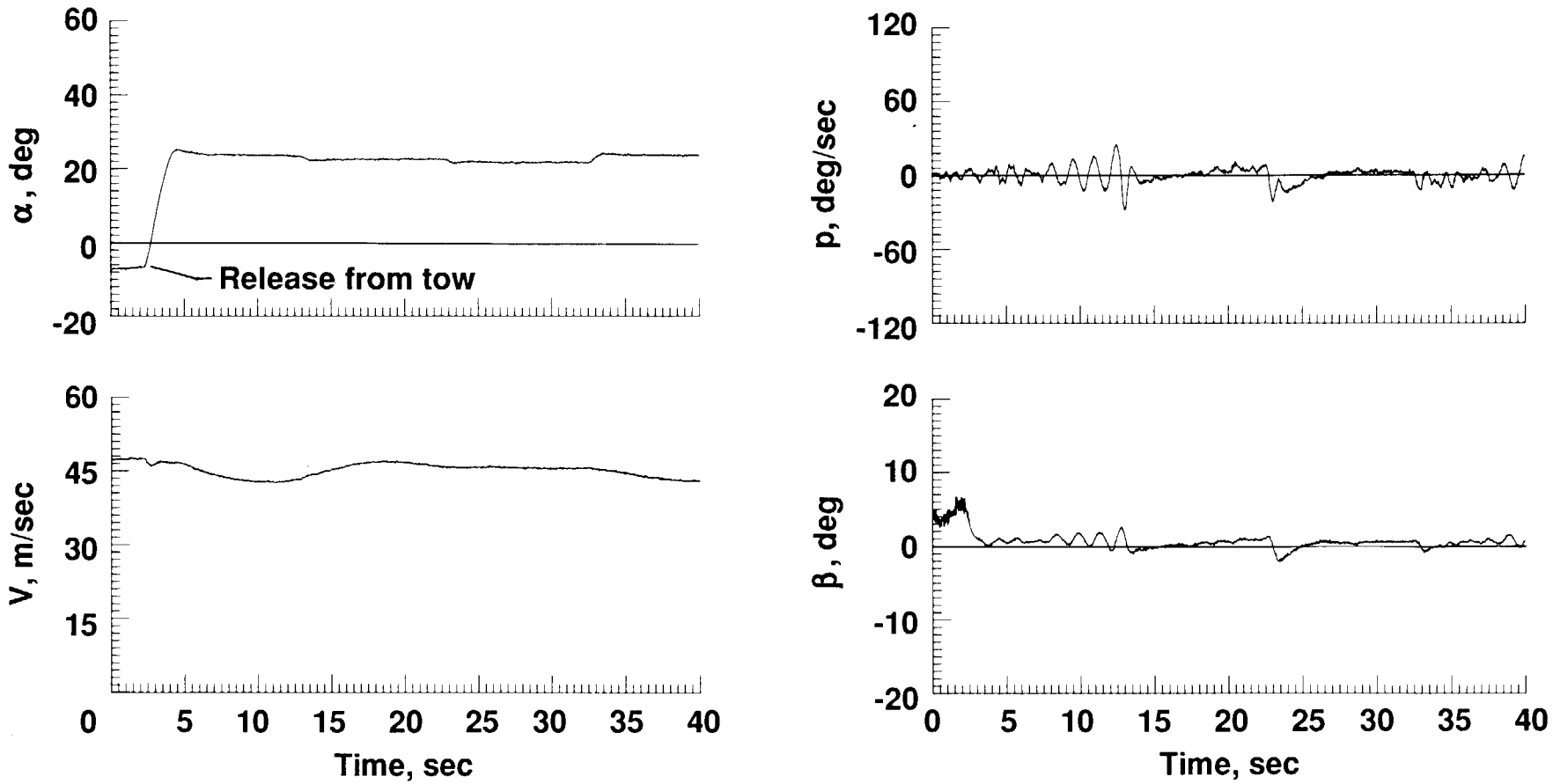

(a) α and V versus time.

(b) p and β versus time.

Figure 3. Time histories for selected input and response variables for the beginning of one of the augmented 1986 flights.

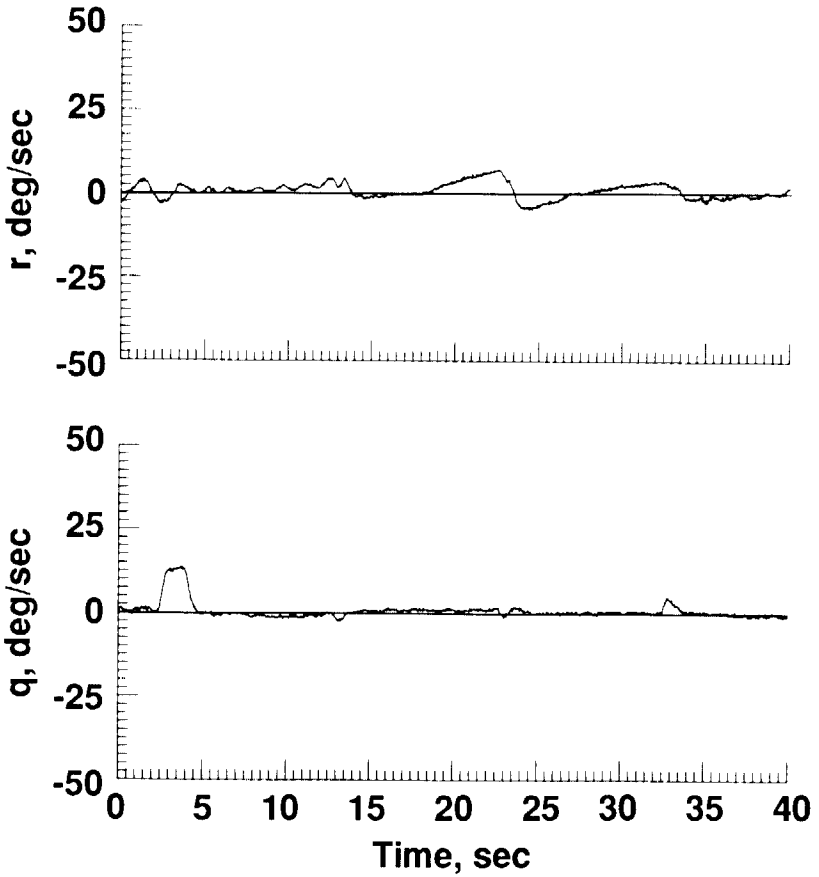

(c) r and q versus time.

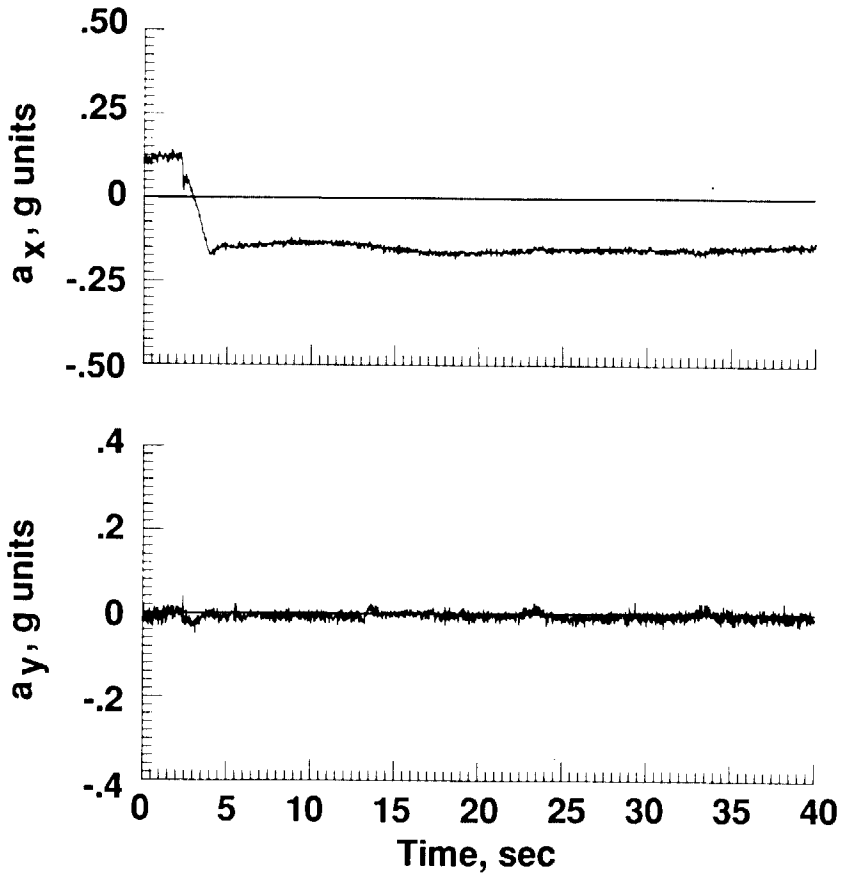

(d) a_x and a_y versus time.

Figure 3. Continued.

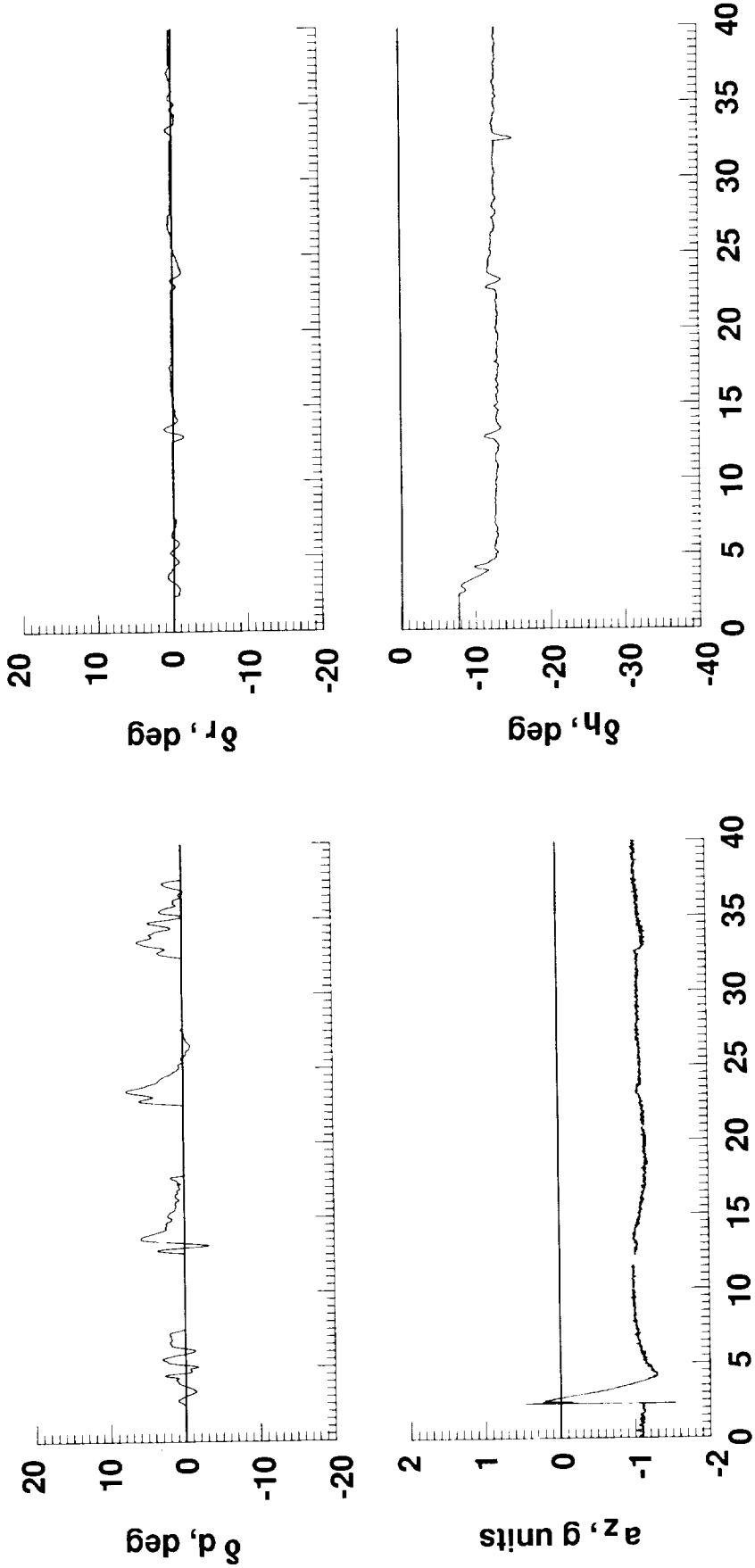

(e) δ_d and a_z versus time.

(f) δ_r and δ_h versus time.

Figure 3. Continued.

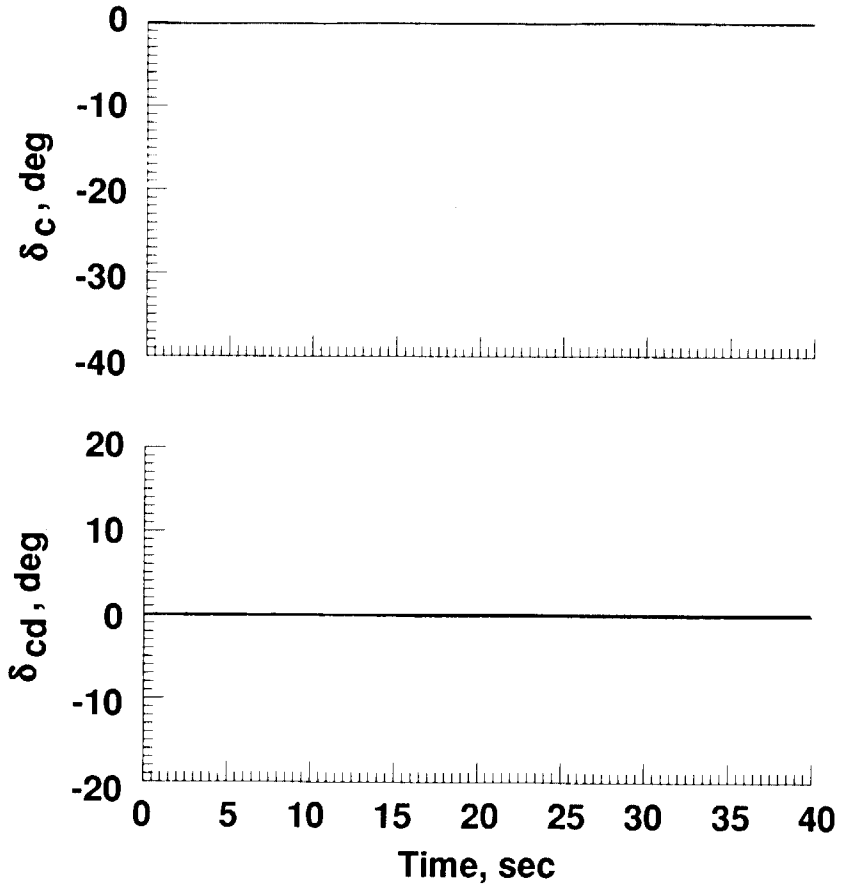

(g) δ_c and δ_{cd} versus time.

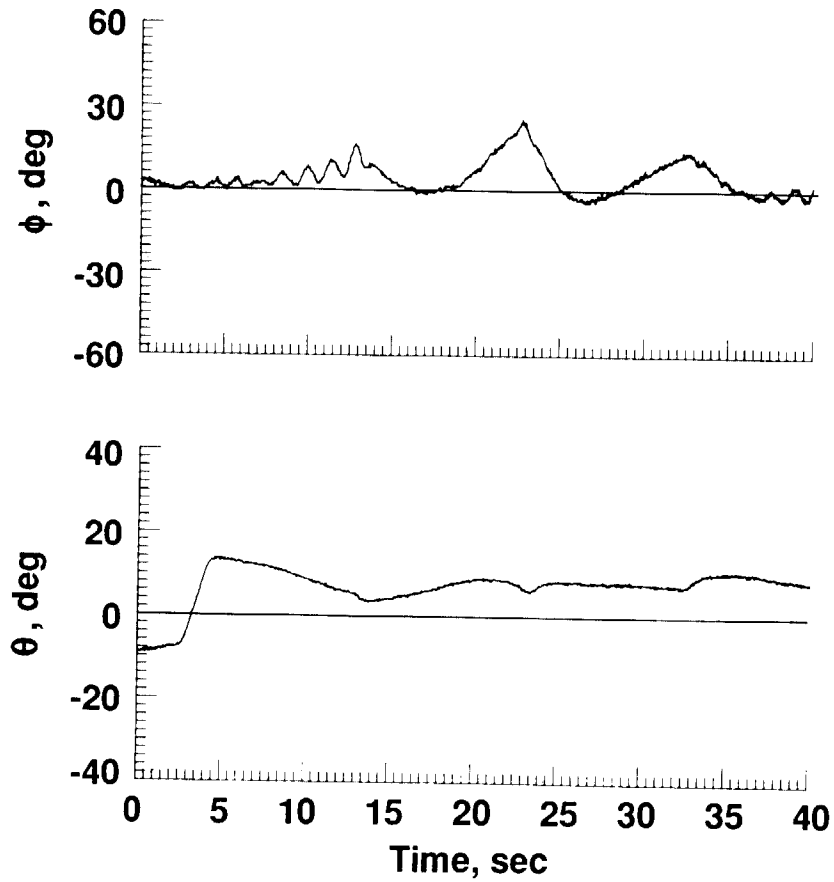

(h) ϕ and θ versus time.

Figure 3. Concluded.

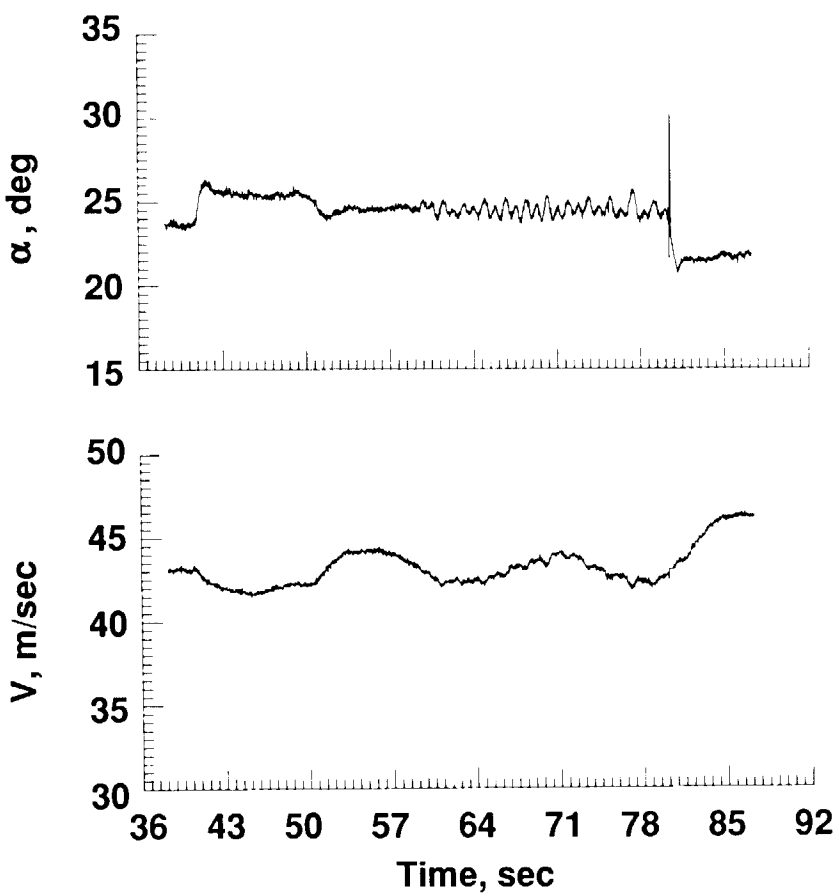

(a) α and V versus time.

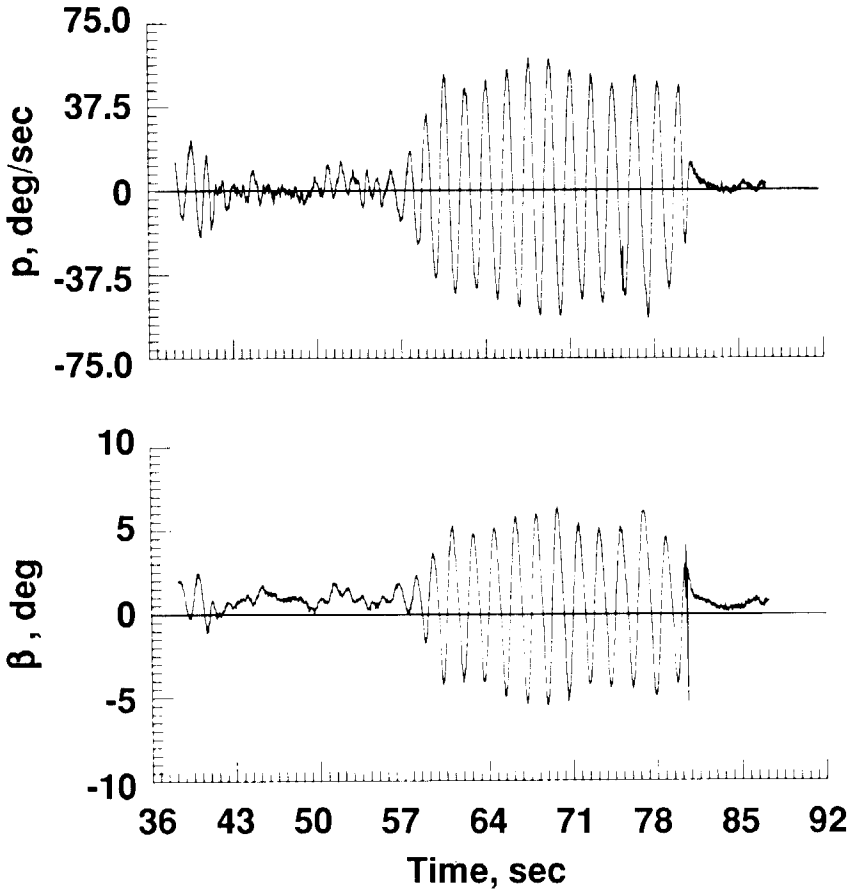

(b) p and β versus time.

Figure 4. Continuation of unaugmented 1983 flight showing spontaneous development of lateral oscillation.

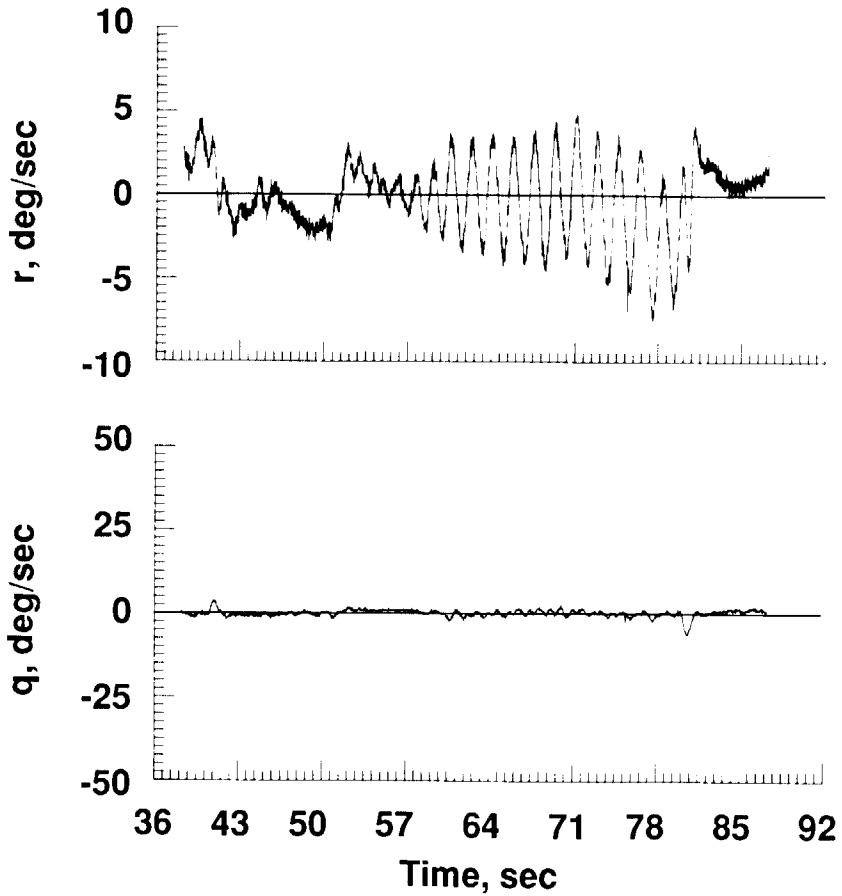

(c) r and q versus time.

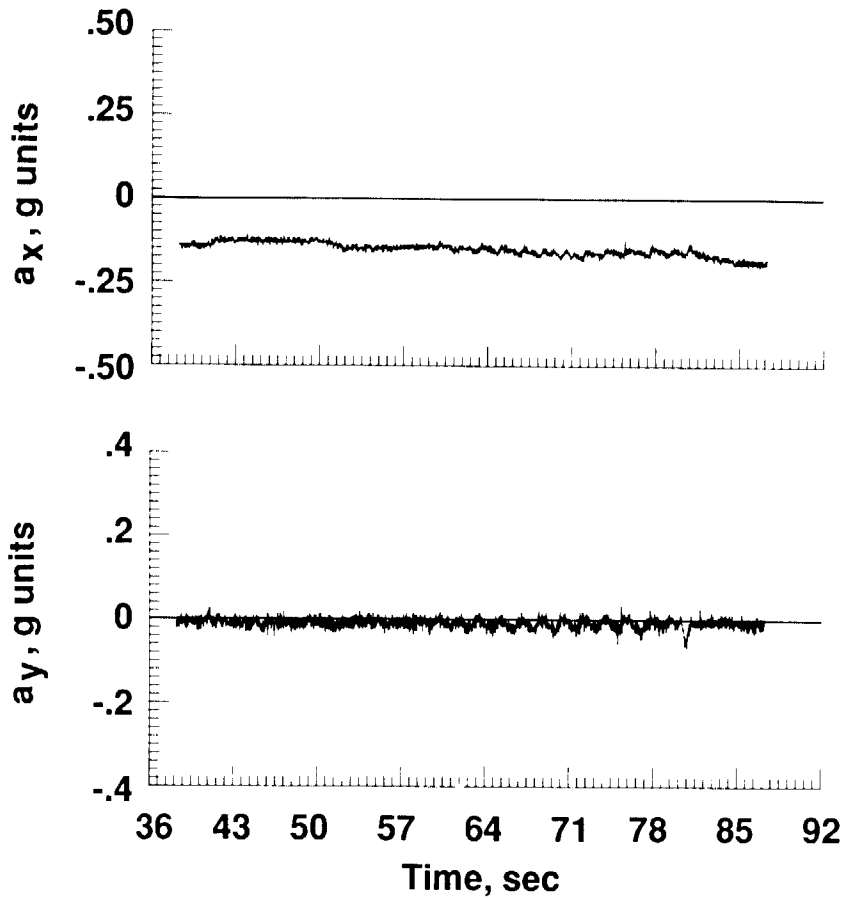

(d) a_x and a_y versus time.

Figure 4. Continued.

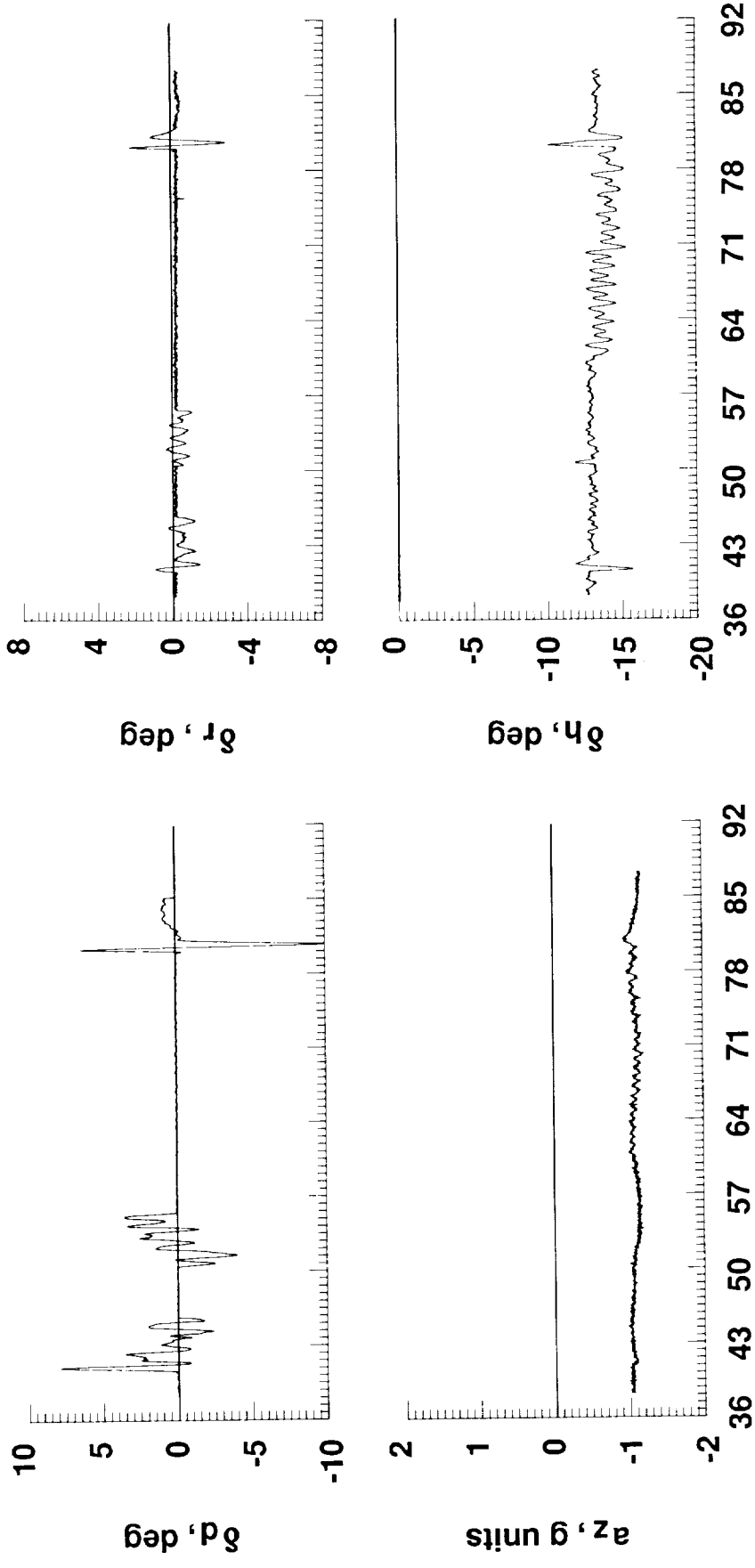

(f) δ_r and δ_h versus time.

(e) δ_d and a_z versus time.

Figure 4. Continued.

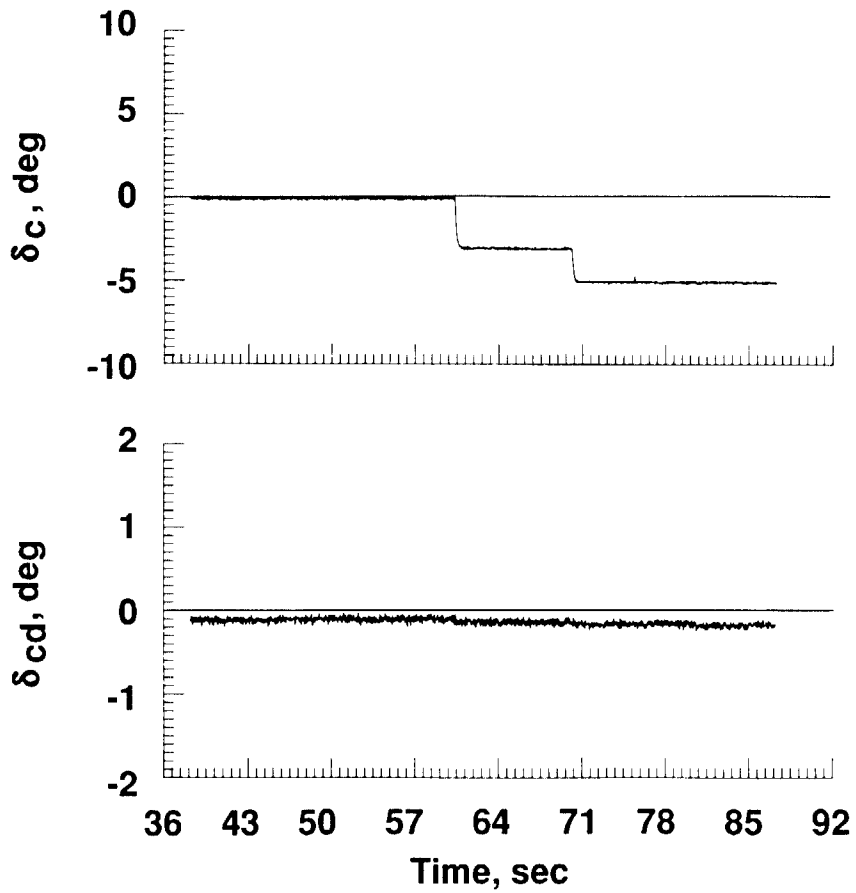

(g) δ_c and δ_{cd} versus time.

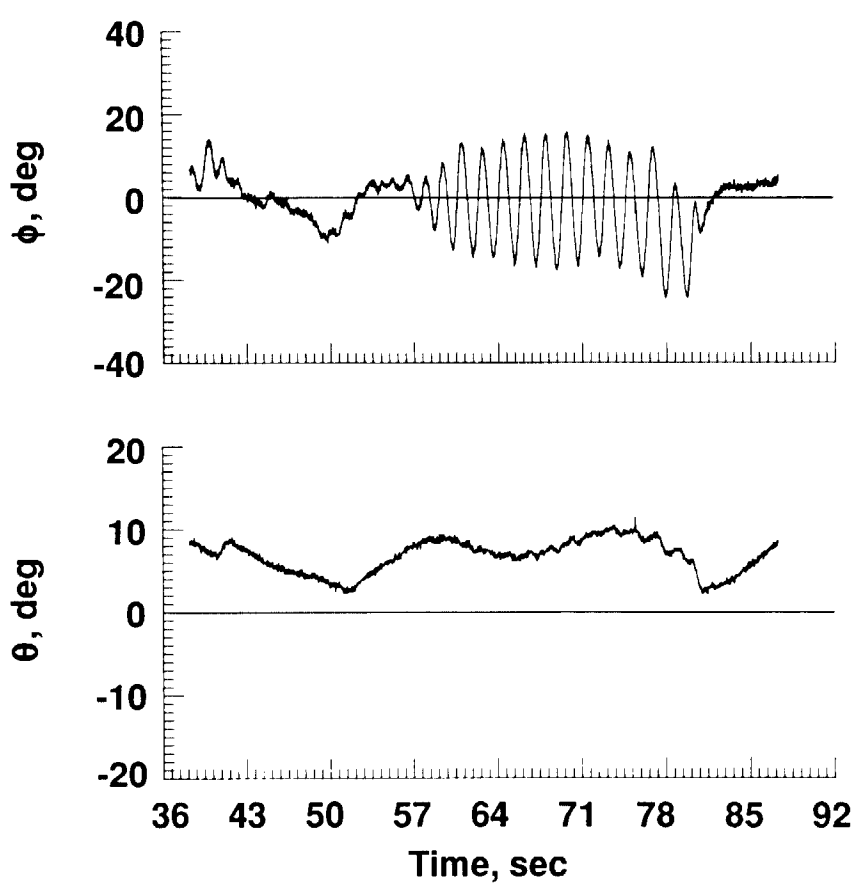

(h) ϕ and θ versus time.

Figure 4. Concluded.

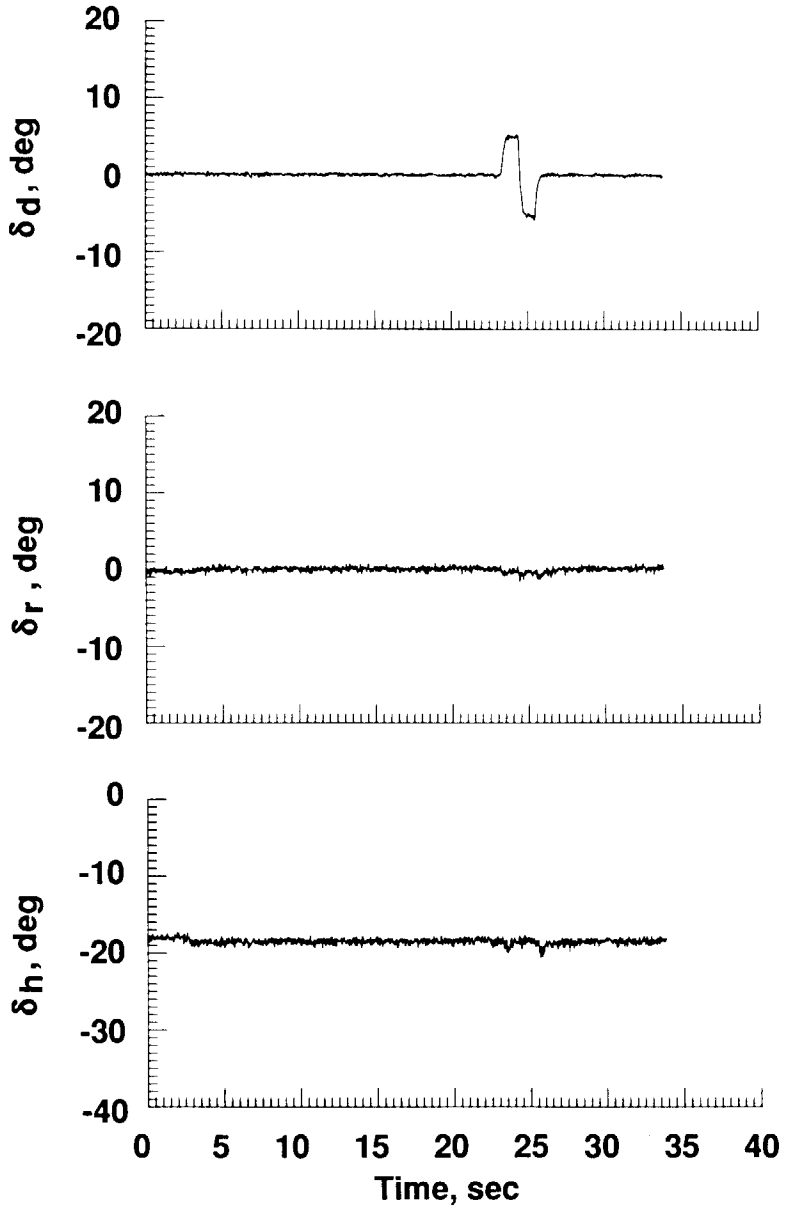

(a) Differential horizontal tail doublet from 1983 test series.

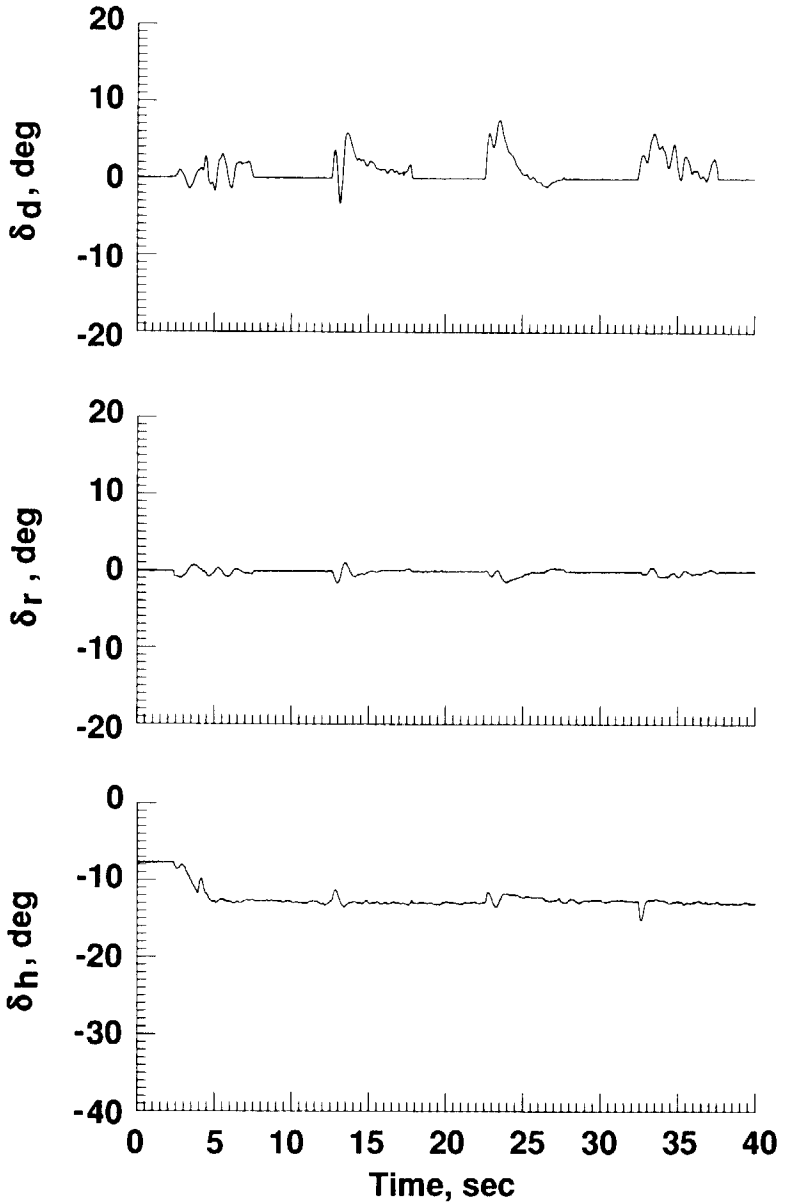

(b) Control surface motion that initiated individual maneuvers for 1986 test series.

Figure 5. Control inputs to initiate individual maneuvers.

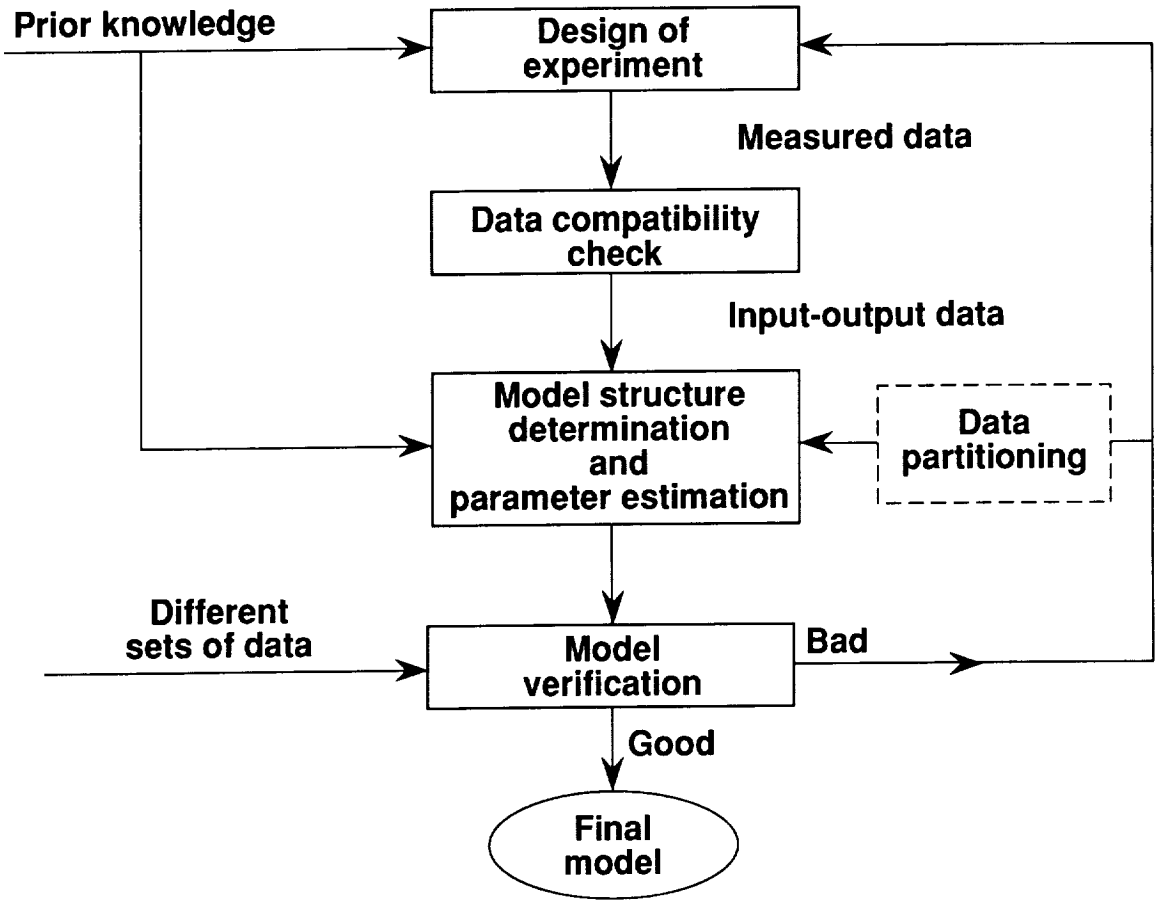

Figure 6. General flow chart for system identification analysis.

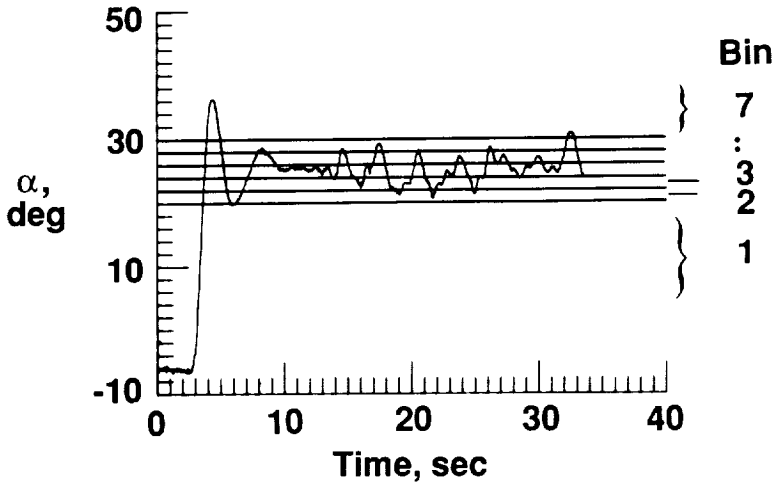

Figure 7. Angle-of-attack time history and partitioning strategy.

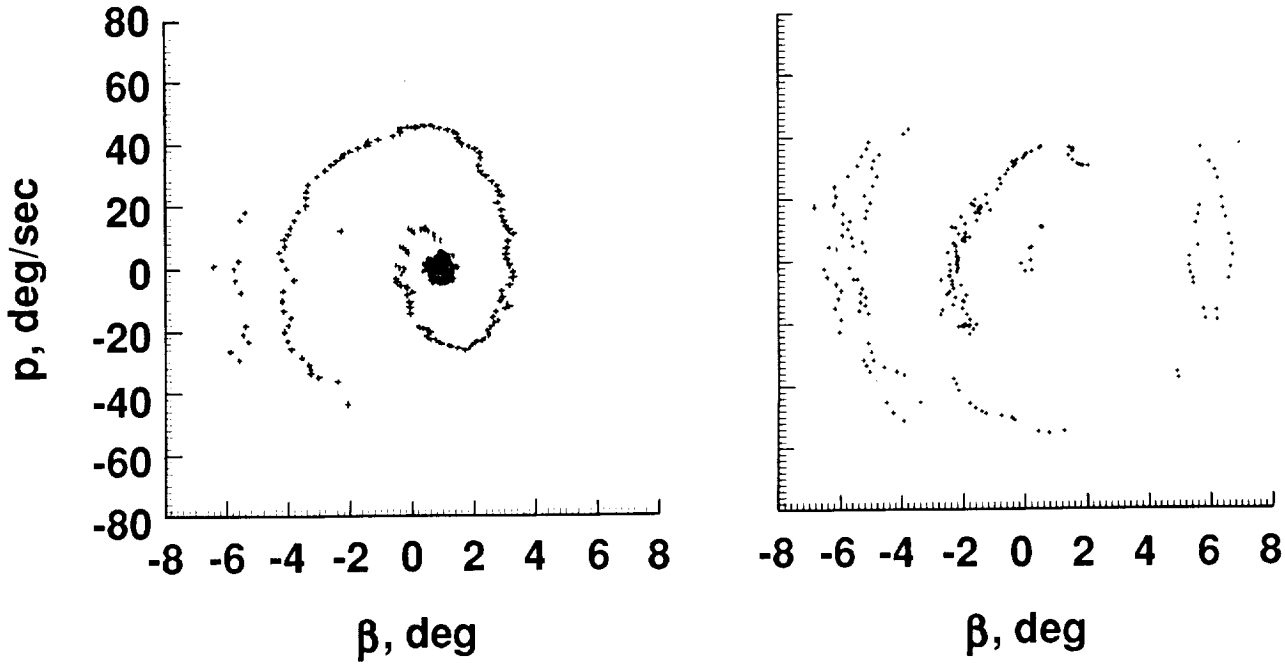

(a) Bin 1.

(b) Bin 2.

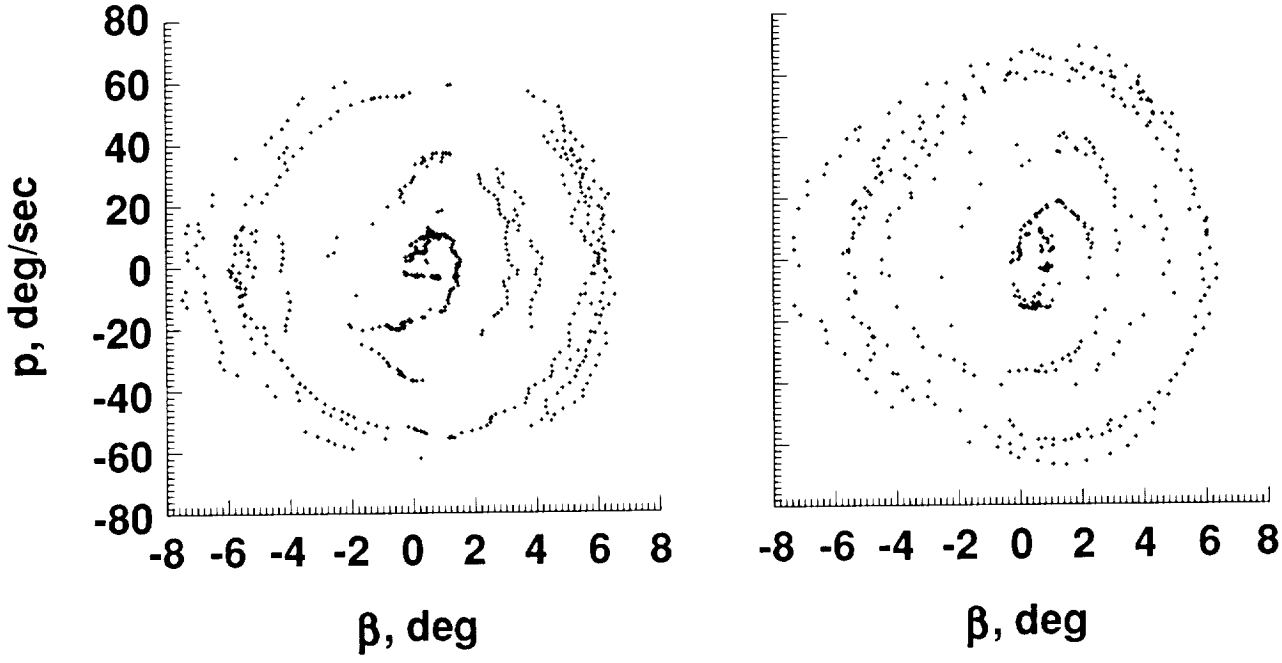

(c) Bin 3.

(d) Bin 4.

Figure 8. Cross plots of roll rate versus sideslip for eight bins after partitioning from one of the 1986 flights.

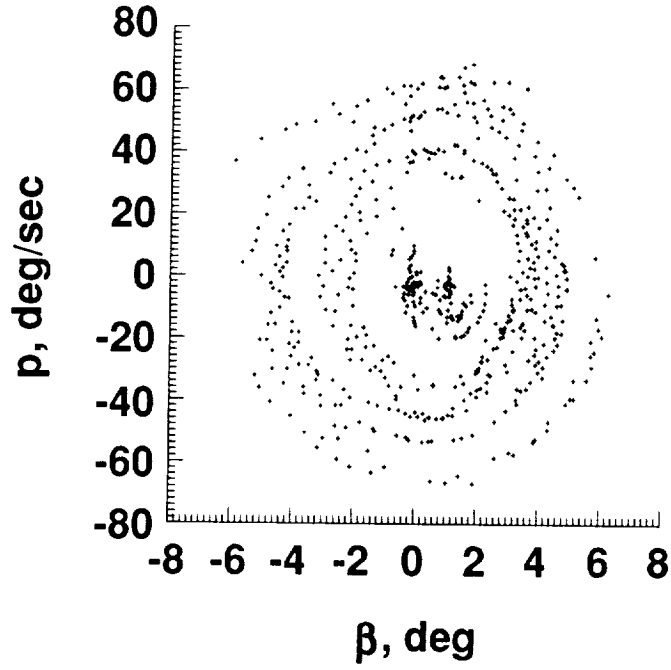

(e) Bin 5.

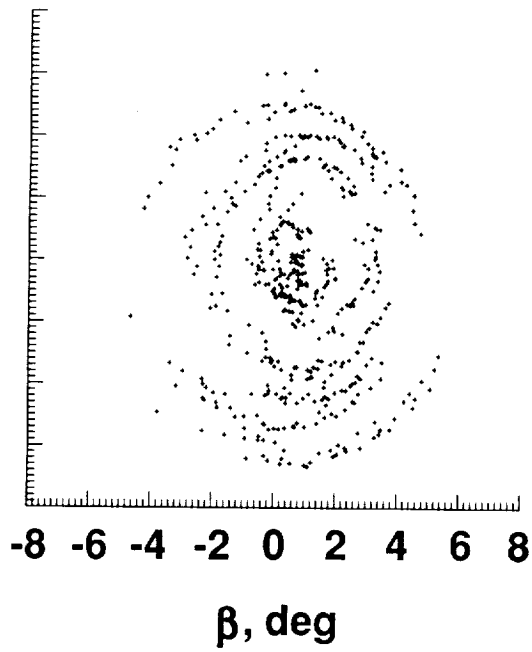

(f) Bin 6.

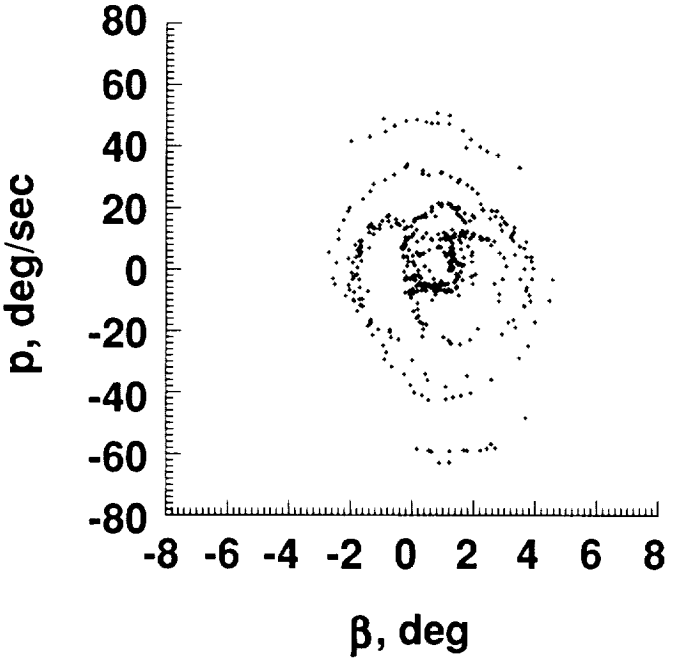

(g) Bin 7.

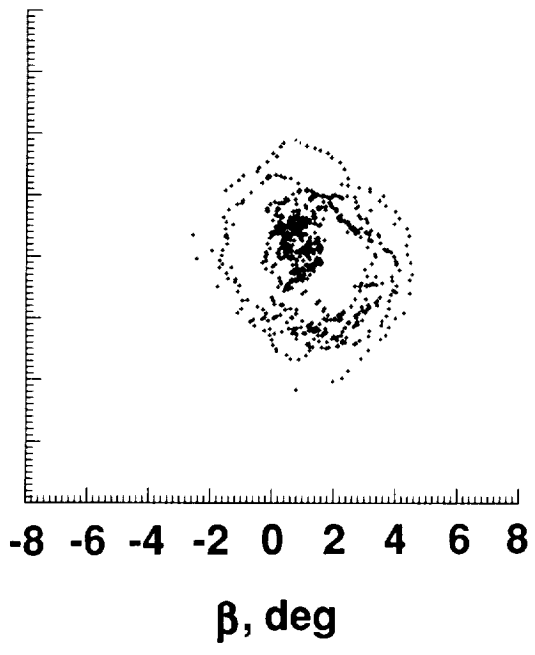

(h) Bin 8.

Figure 8. Concluded.

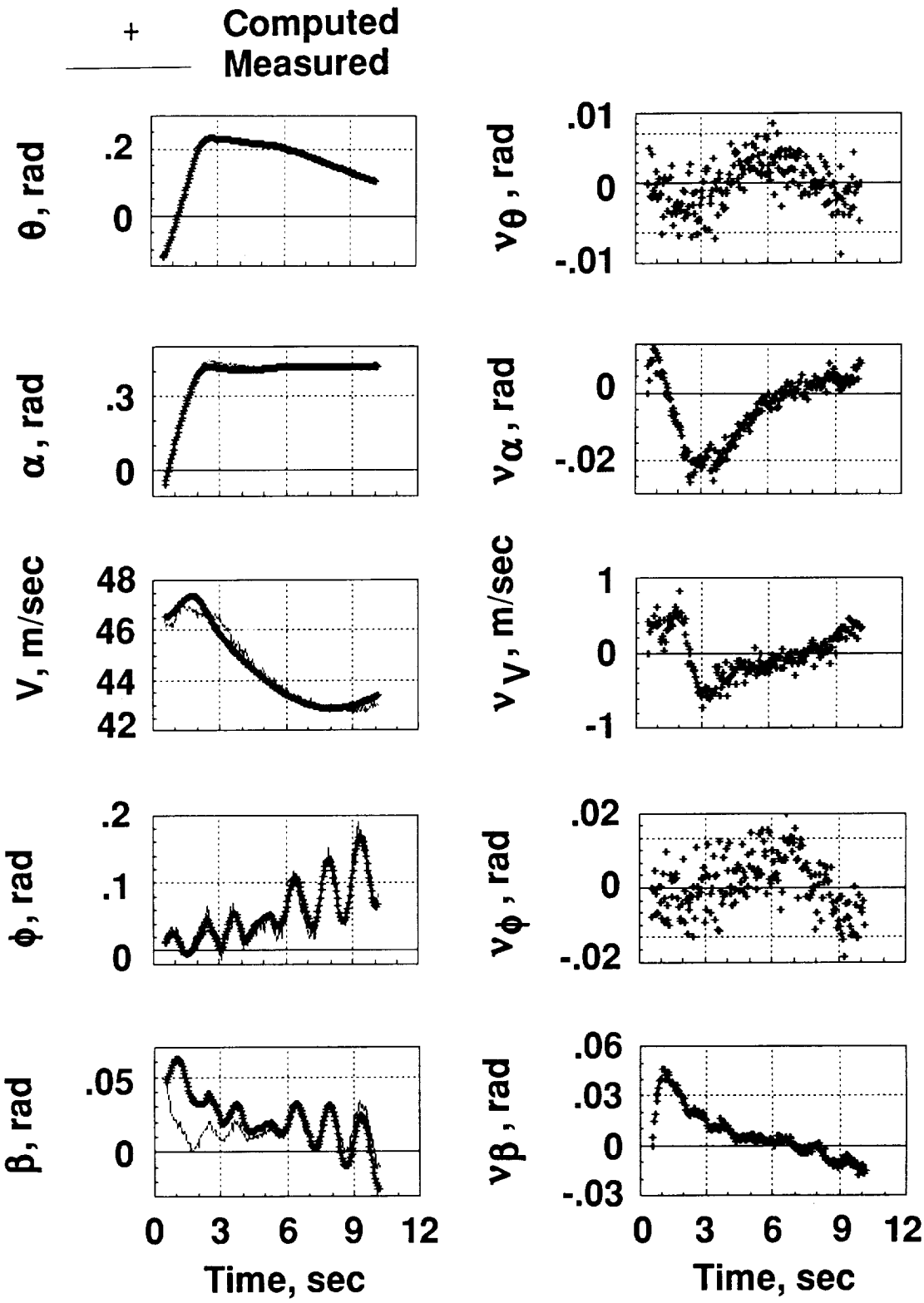

(a) Measured and computed time histories.

(b) Residual time histories.

Figure 9. Results of compatibility check.

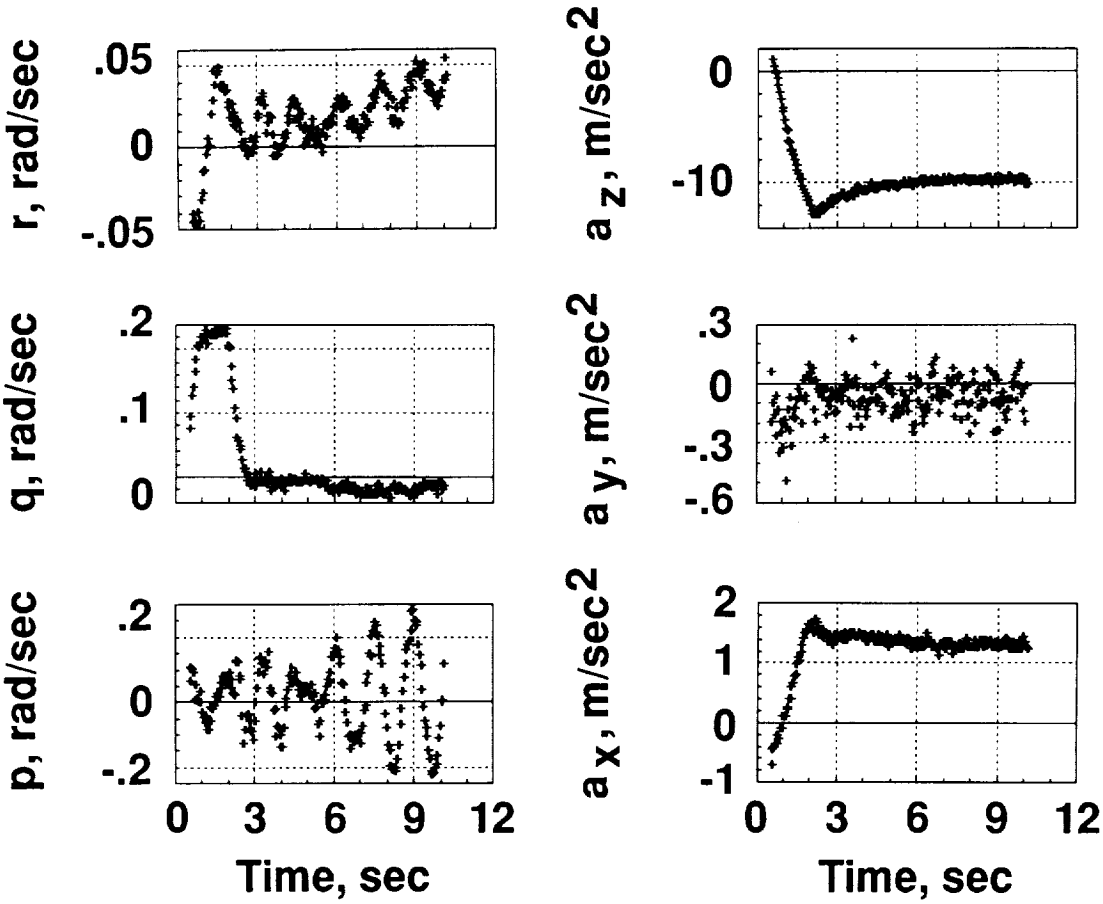

(c) Input time histories.

Figure 9. Concluded.

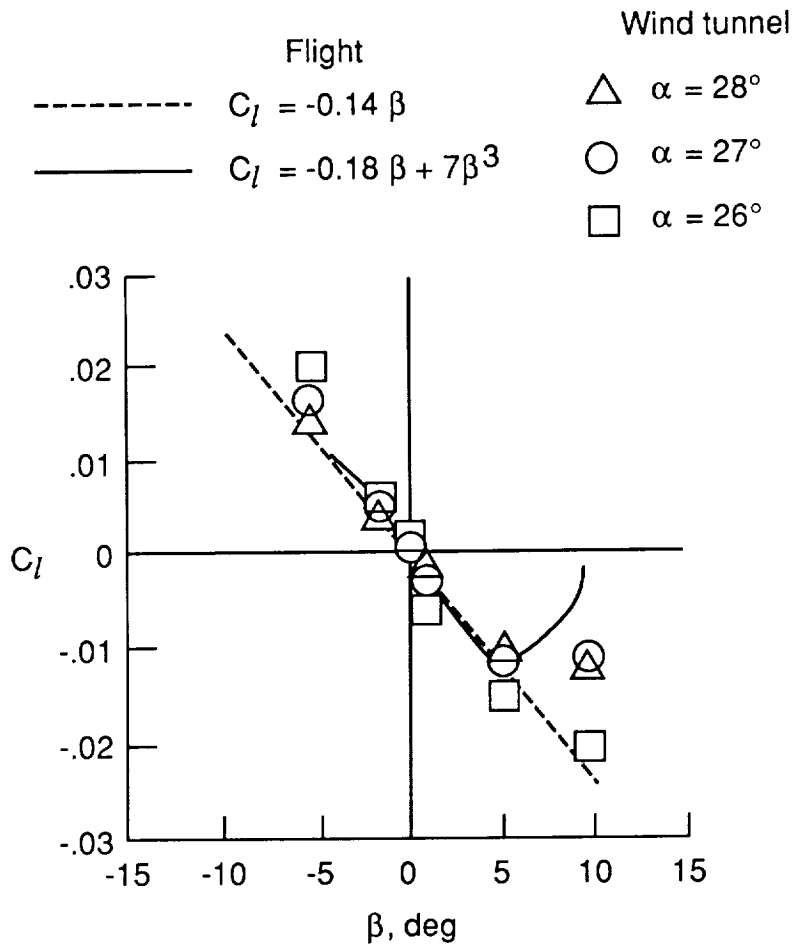

Figure 10. Nonlinear dependence of rolling-moment coefficient on angle of sideslip with $\delta_c = 0°$.

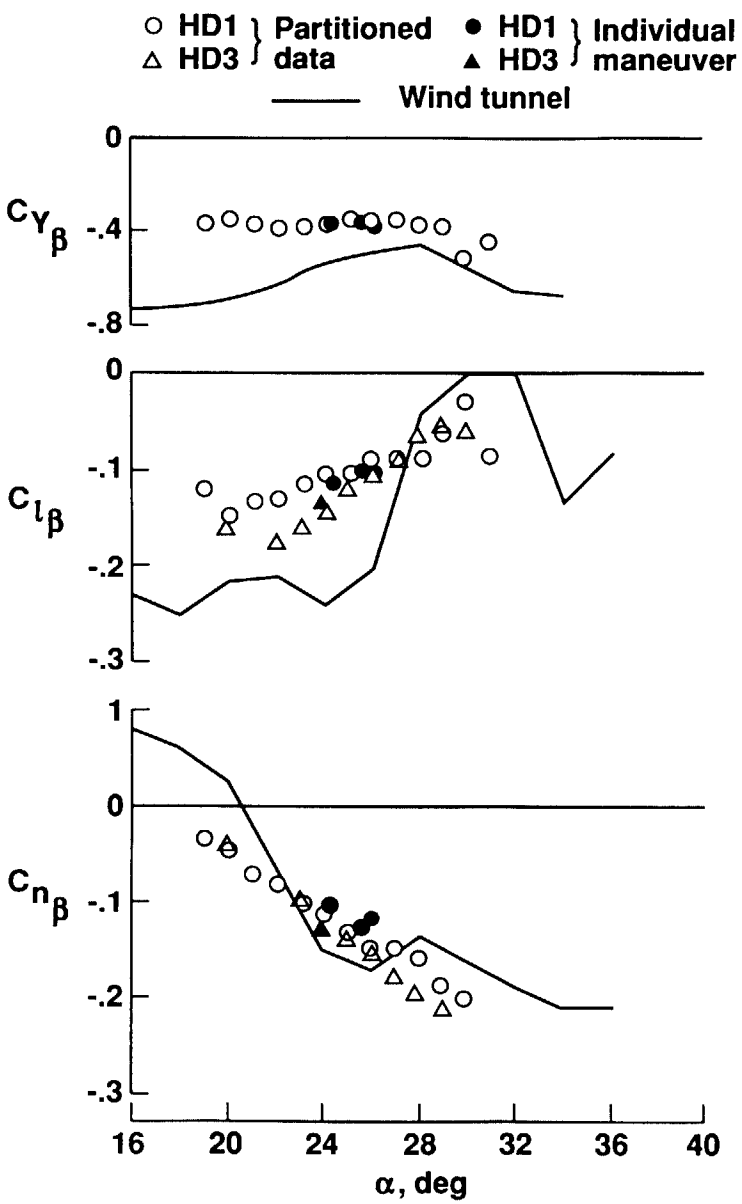

(a) 1983 flights with $\delta_c = 10°$.

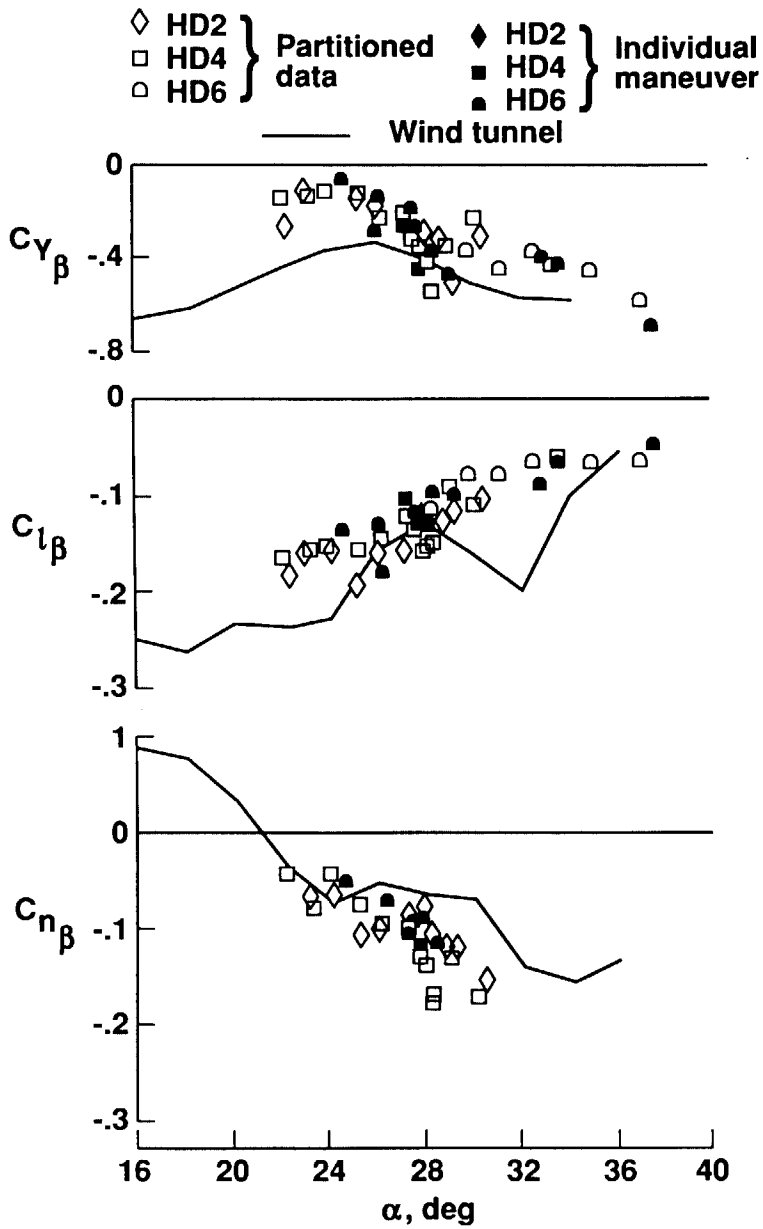

(b) 1983 flights with $\delta_c = 0°$.

Figure 11. Sideslip derivatives.

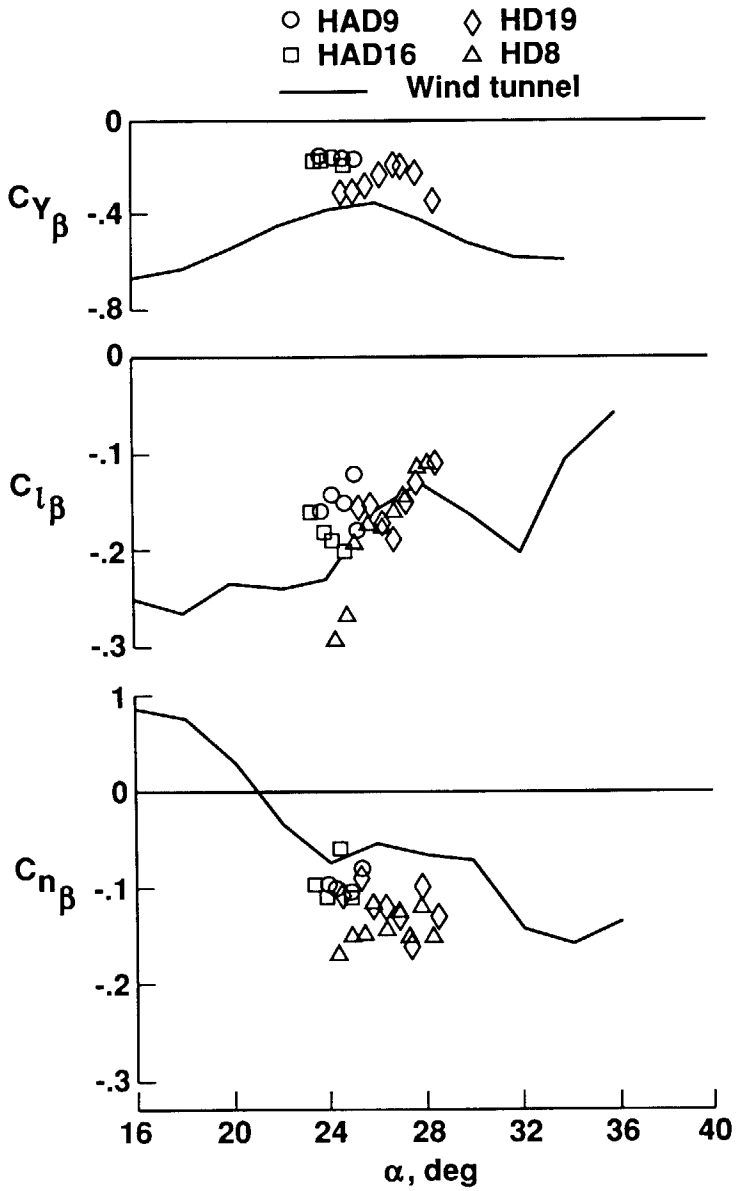

(c) 1986 flights with $\delta_c = 0°$.

Figure 11. Concluded.

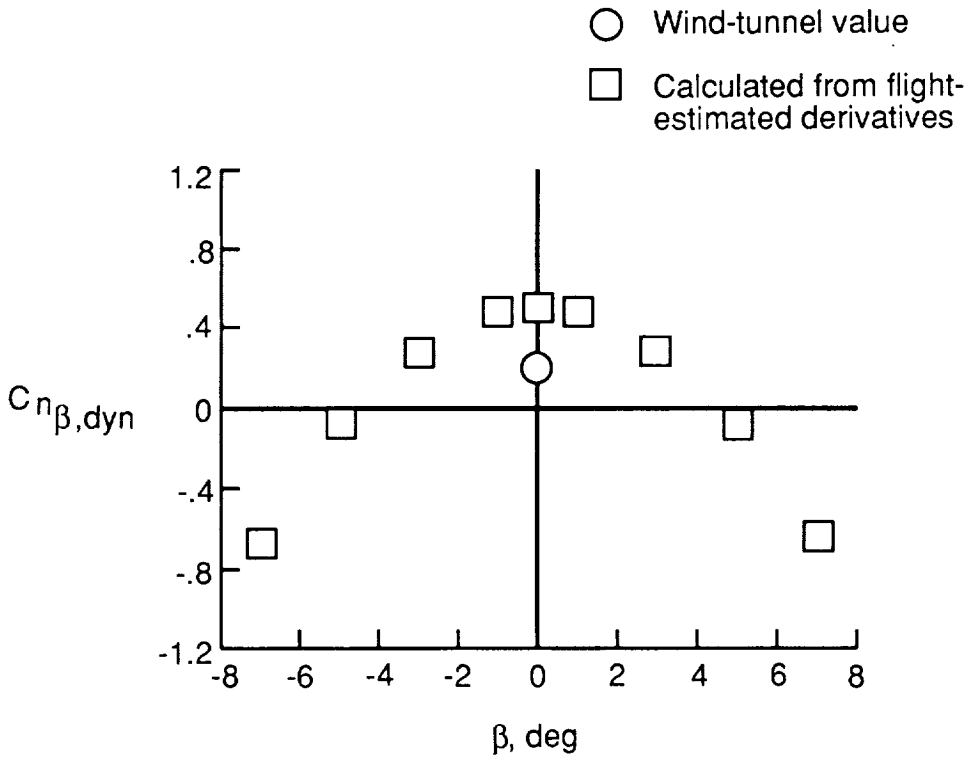

Figure 12. Variation of $C_{n_{\beta,\mathrm{dyn}}}$ with β for $\alpha = 25°$.

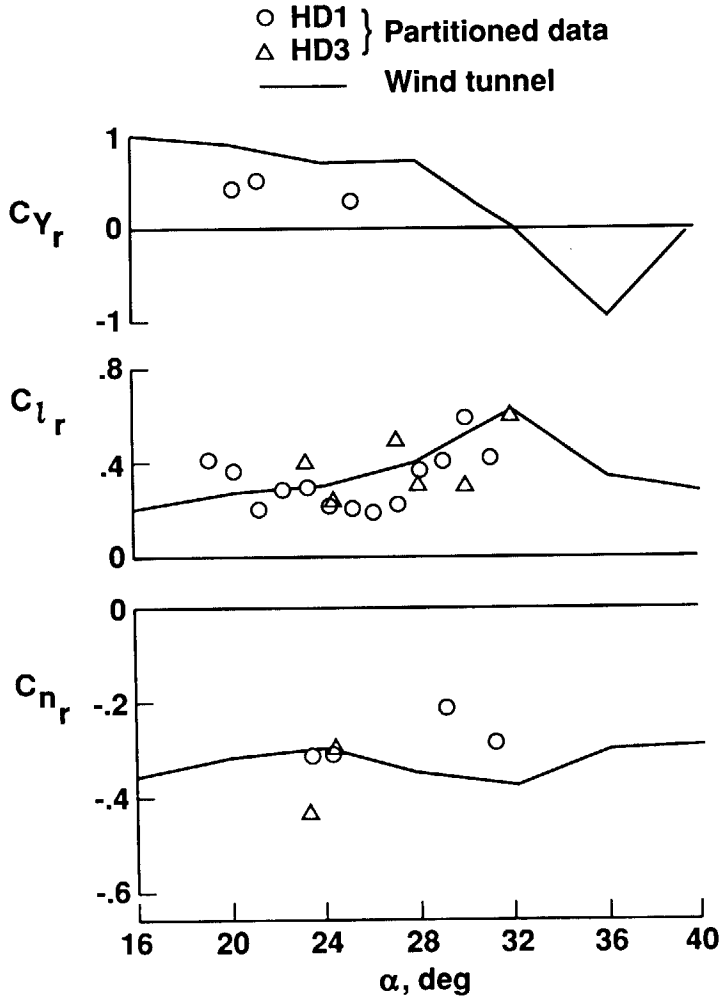

(a) 1983 flights with $\delta_c = -10°$.

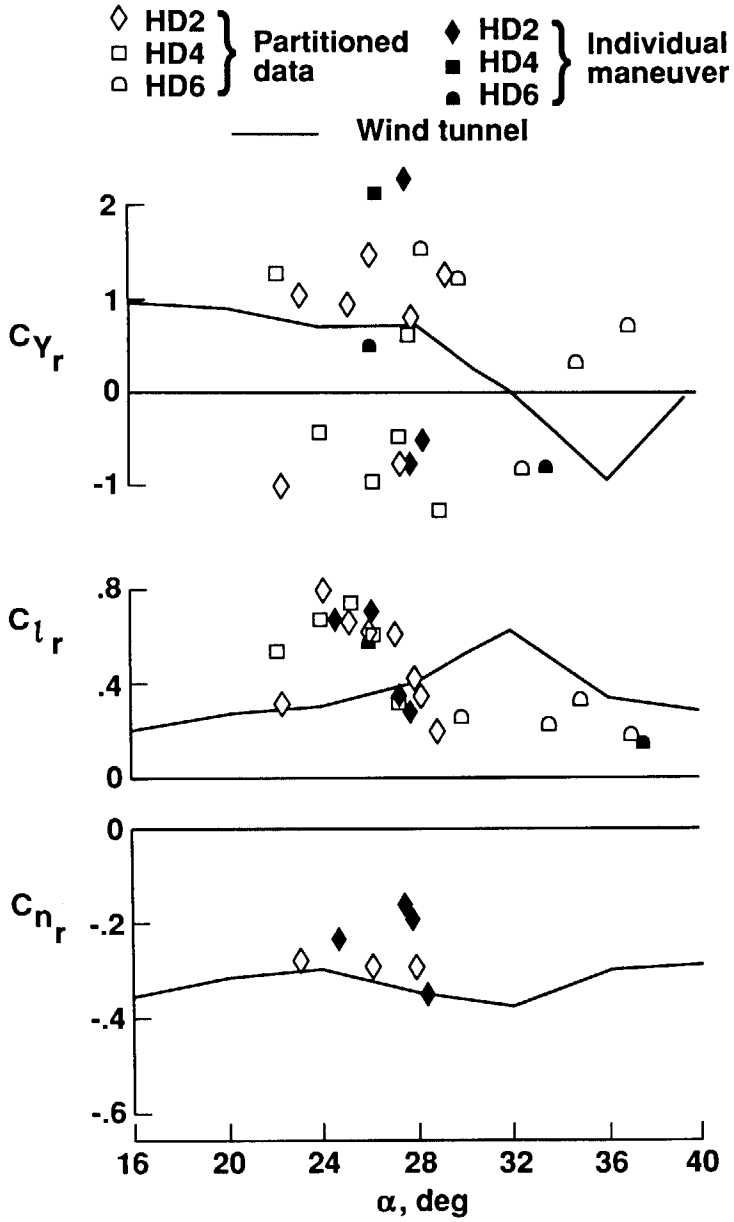

(b) 1983 flights with $\delta_c = 0°$.

Figure 13. Yaw rate derivatives.

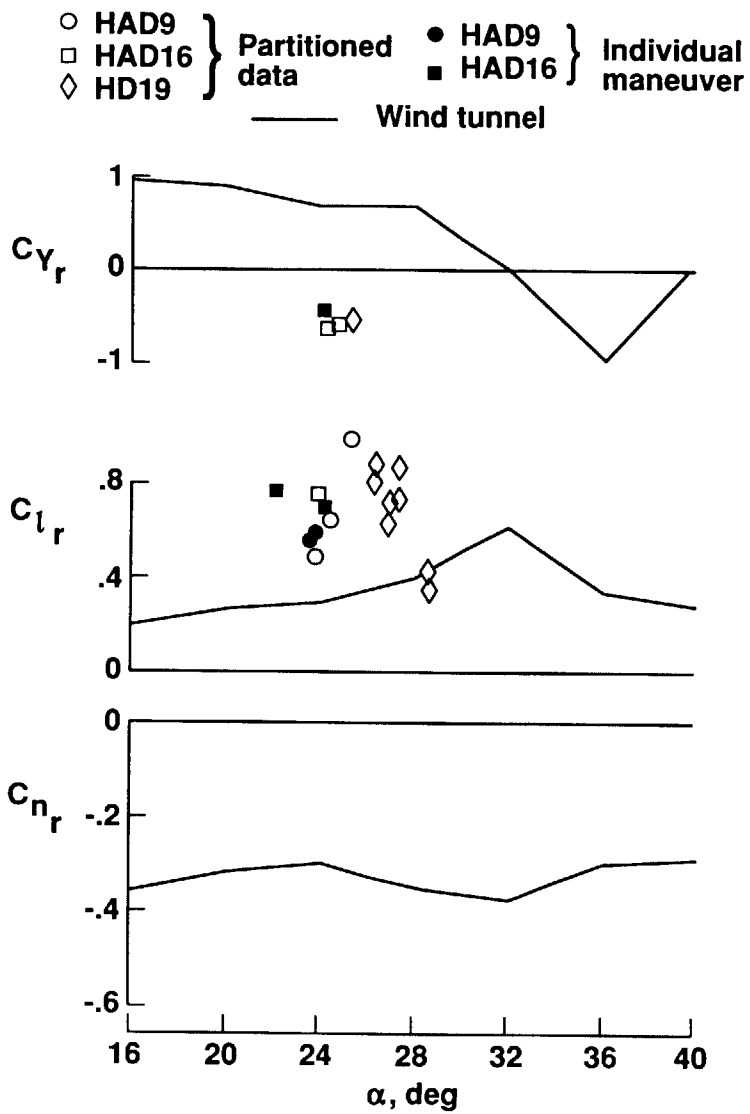

(c) 1986 flights.

Figure 13. Concluded.

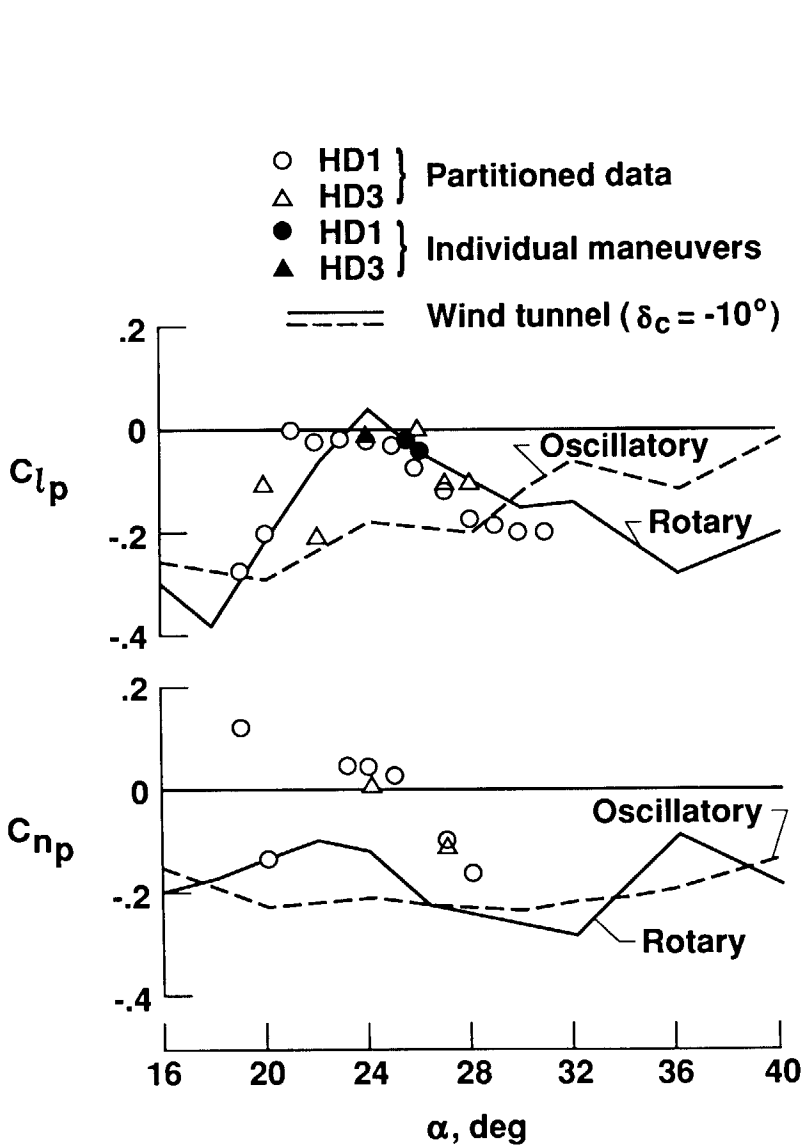

(a) 1983 flights with $\delta_c = -10°$.

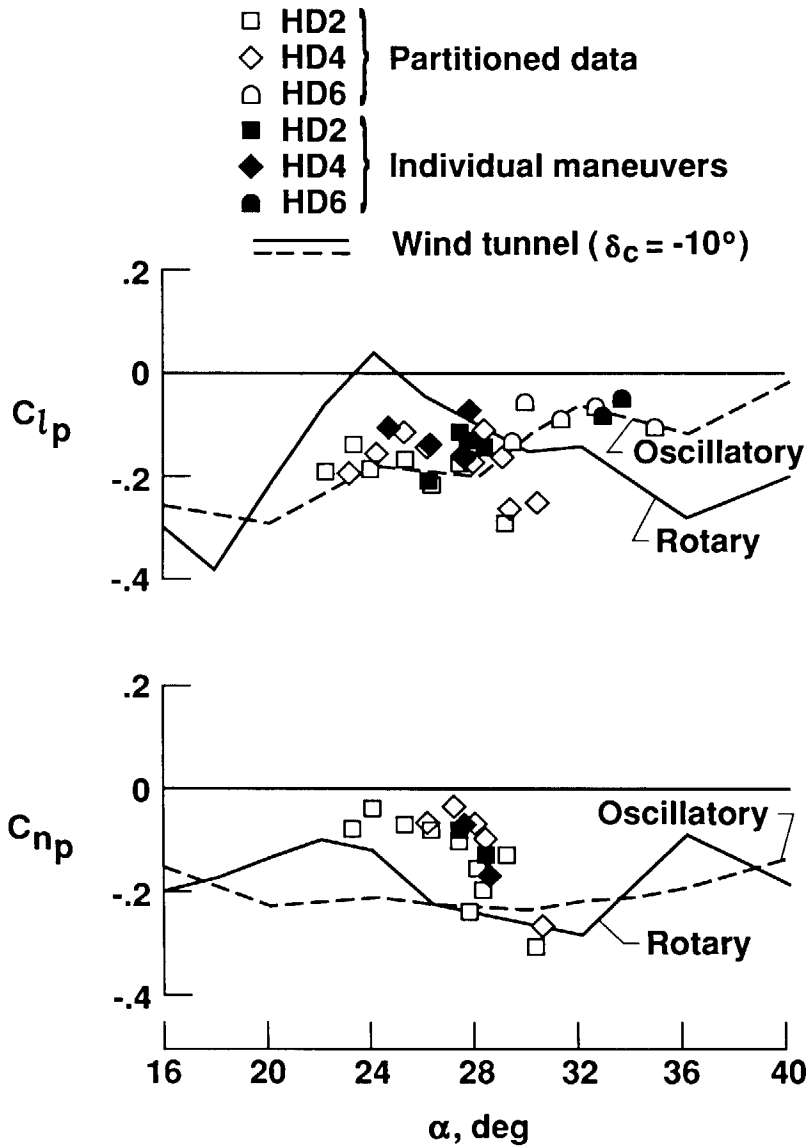

(b) 1983 flights with $\delta_c = 0°$.

Figure 14. Roll rate derivatives.

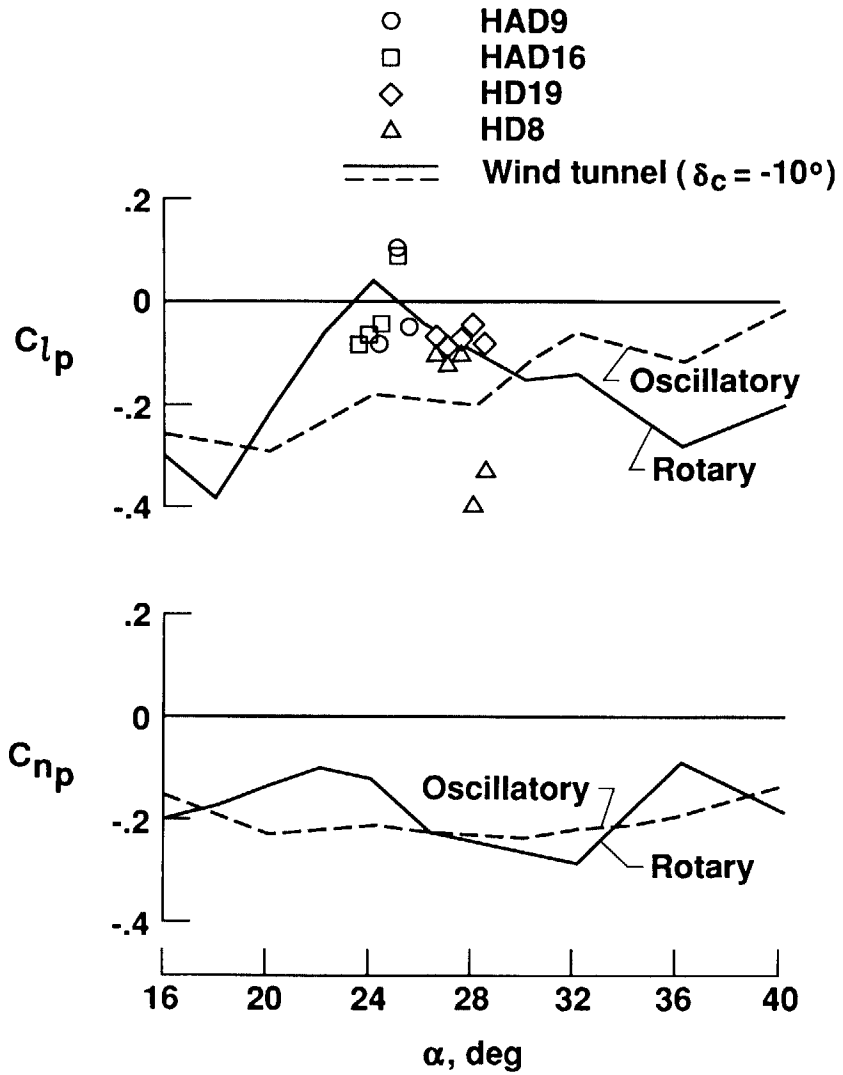

(c) 1986 flights.

Figure 14. Concluded.

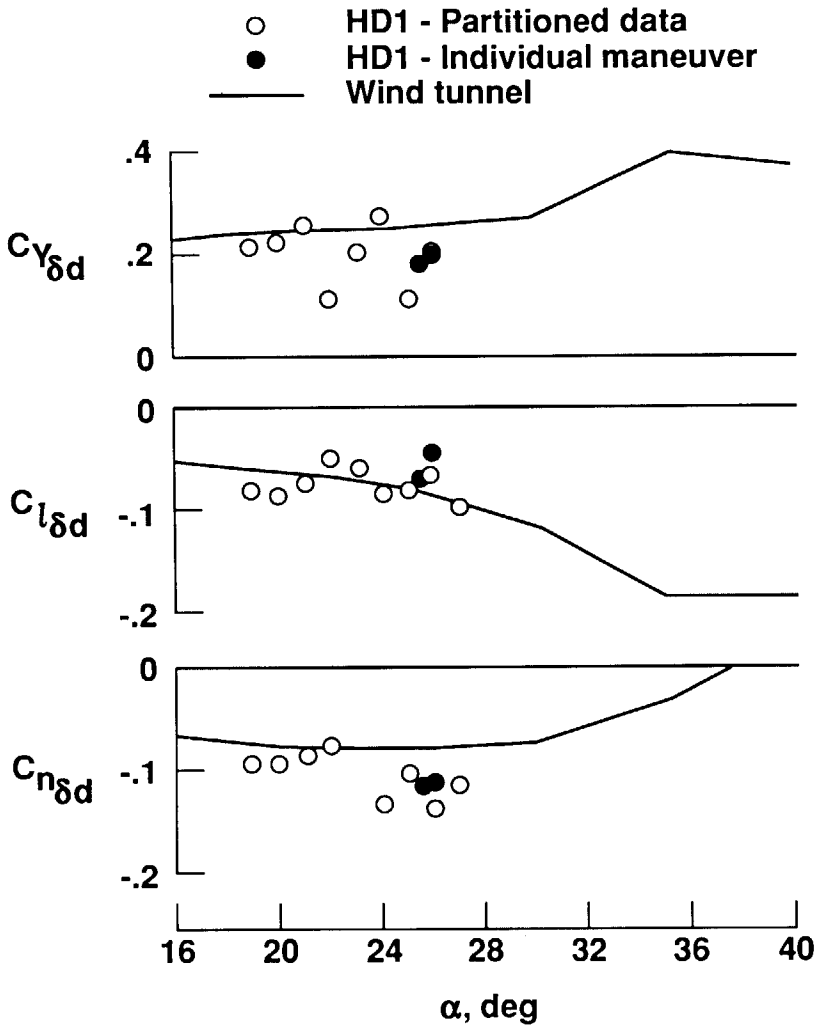

(a) 1983 flights with $\delta_c = -10°$

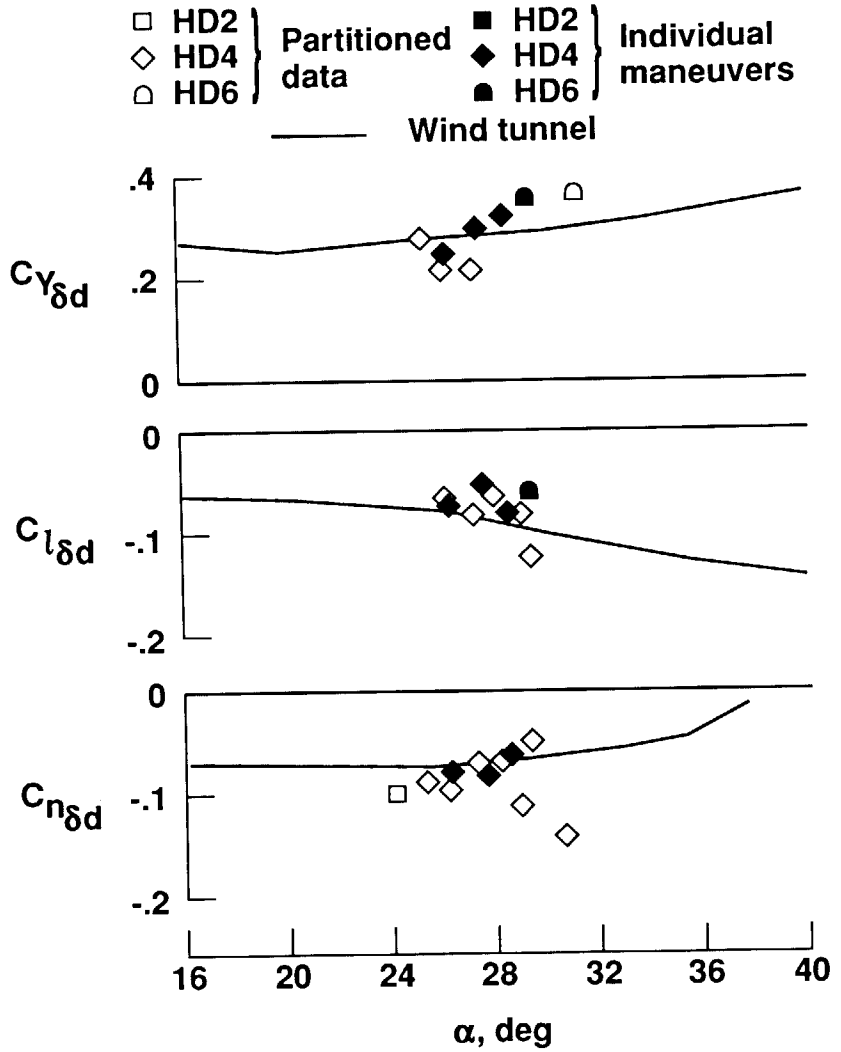

(b) 1983 flights with $\delta_c = 0°$.

Figure 15. Differential tail derivatives.

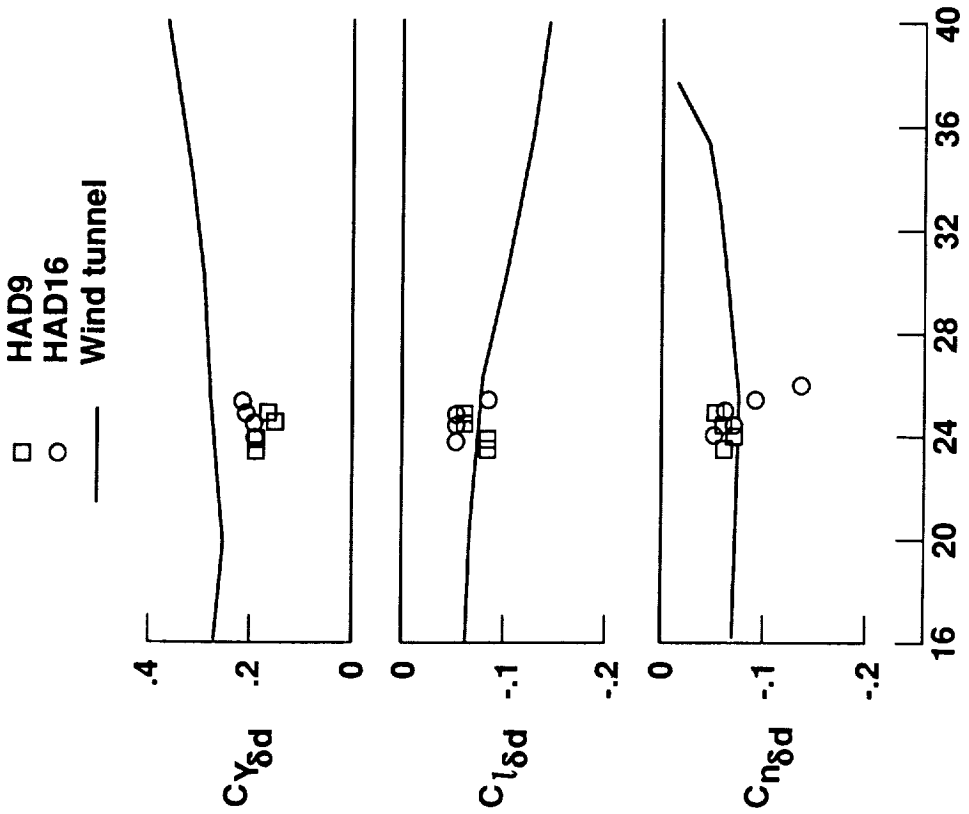

(c) 1986 flights.

Figure 15. Concluded.

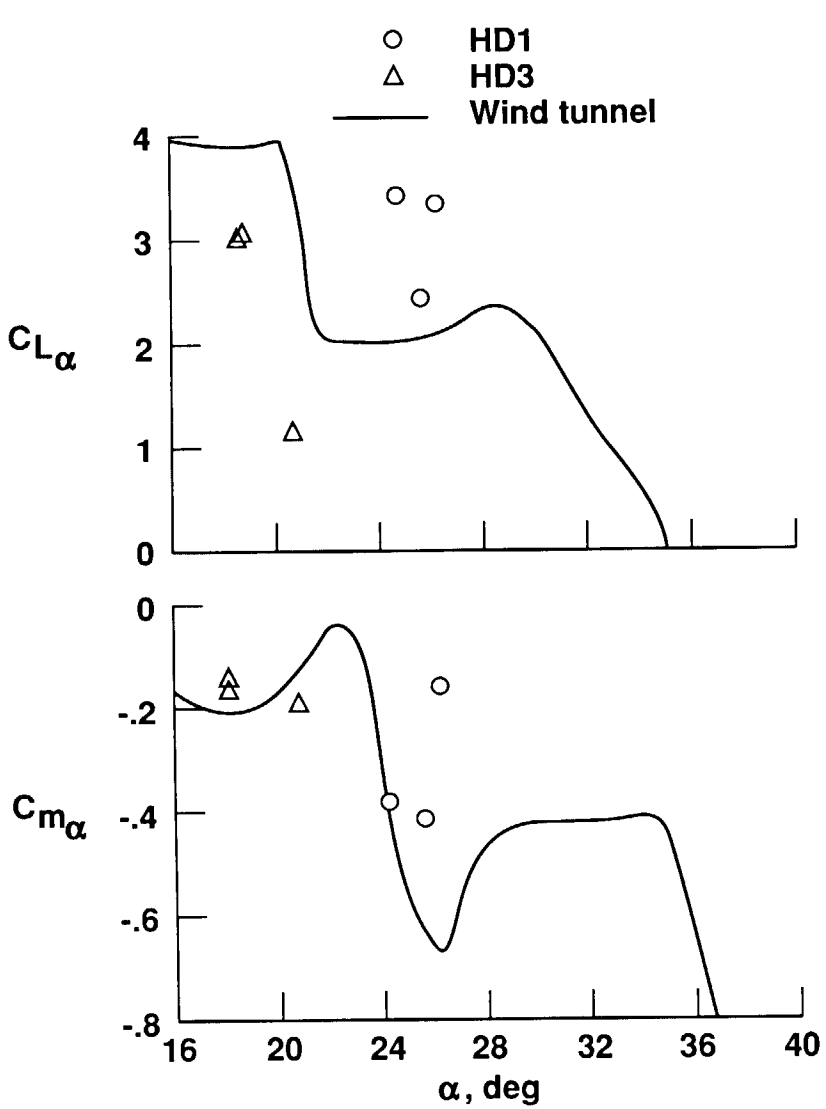

(a) 1983 flights.

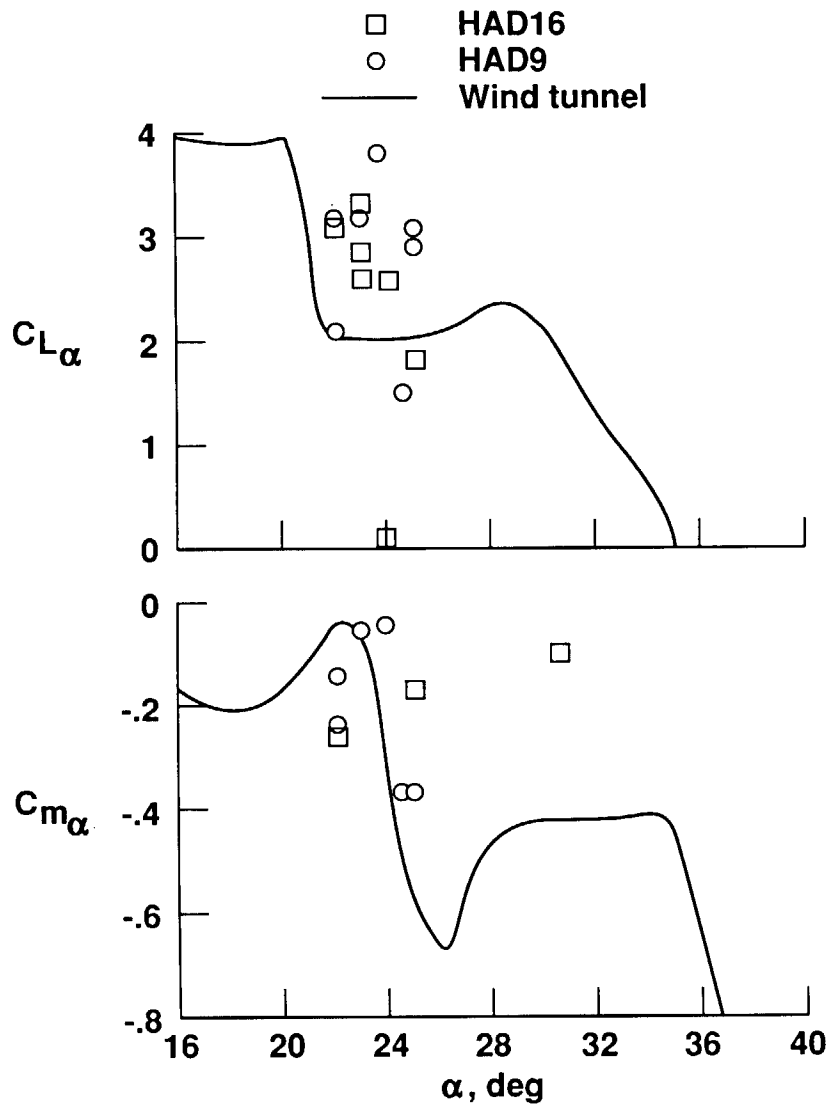

(b) 1986 flights.

Figure 16. Slopes of lift and pitching-moment coefficients.

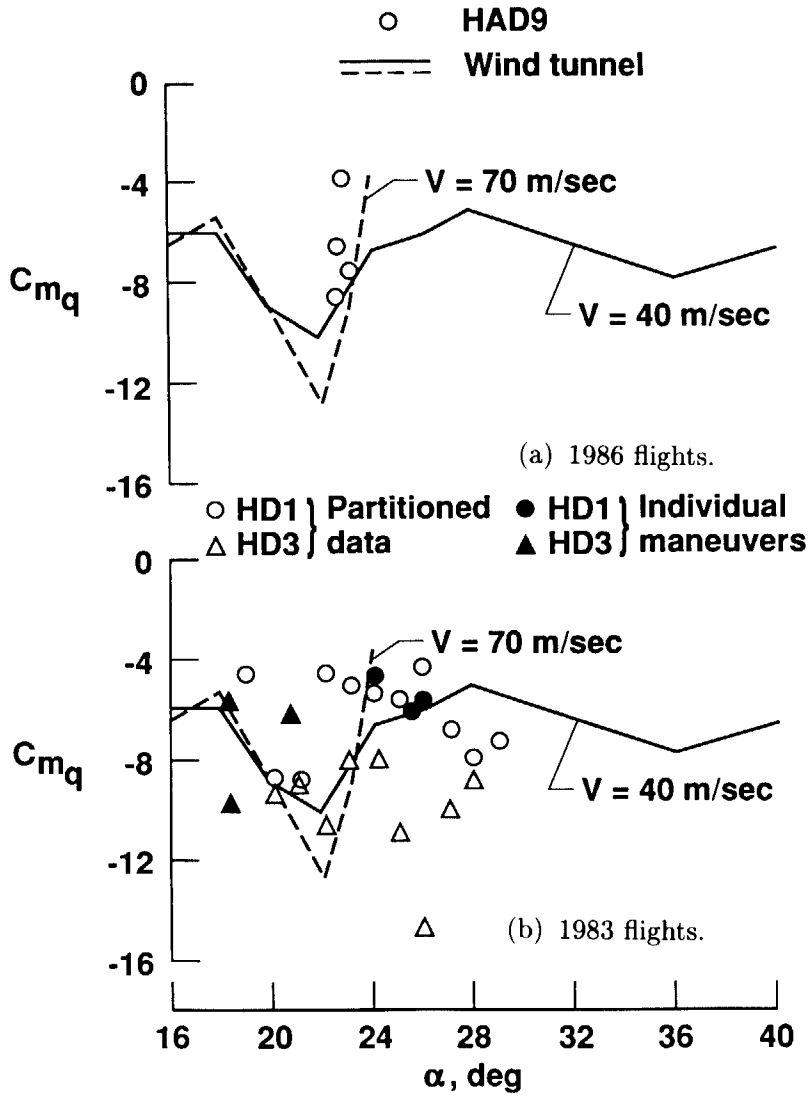

Figure 17. Pitch rate derivatives.

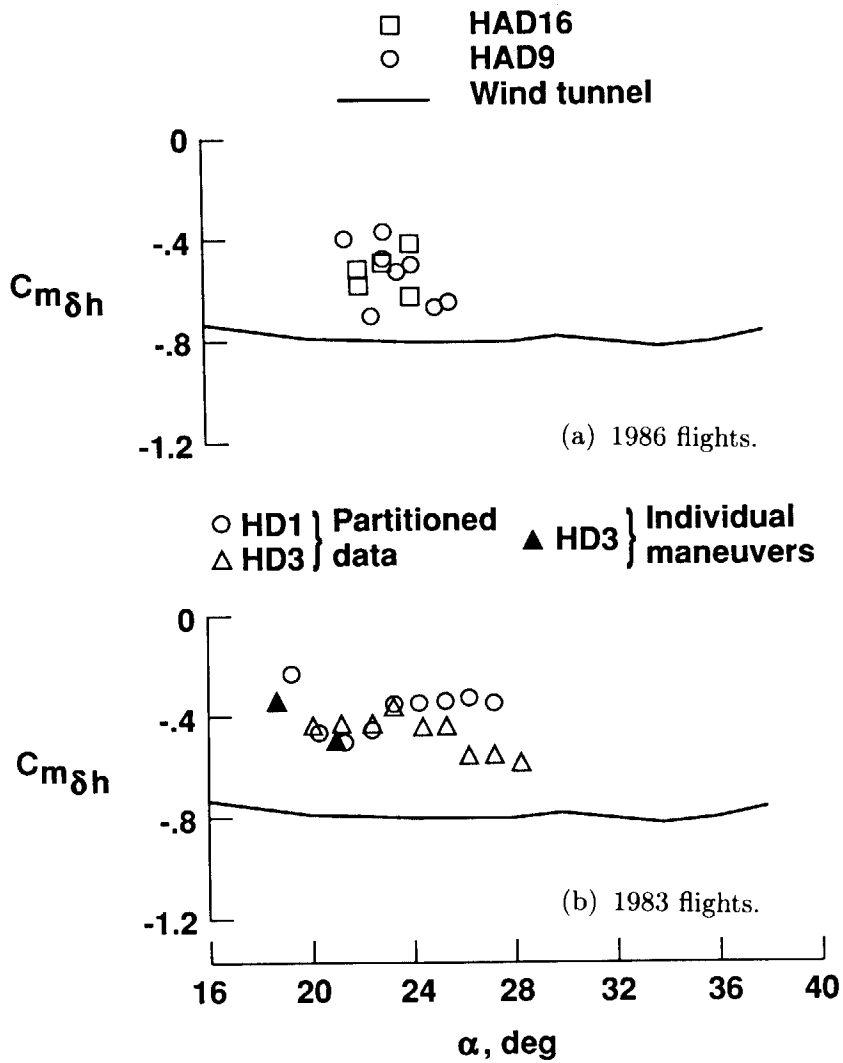

Figure 18. Horizontal tail effectiveness.

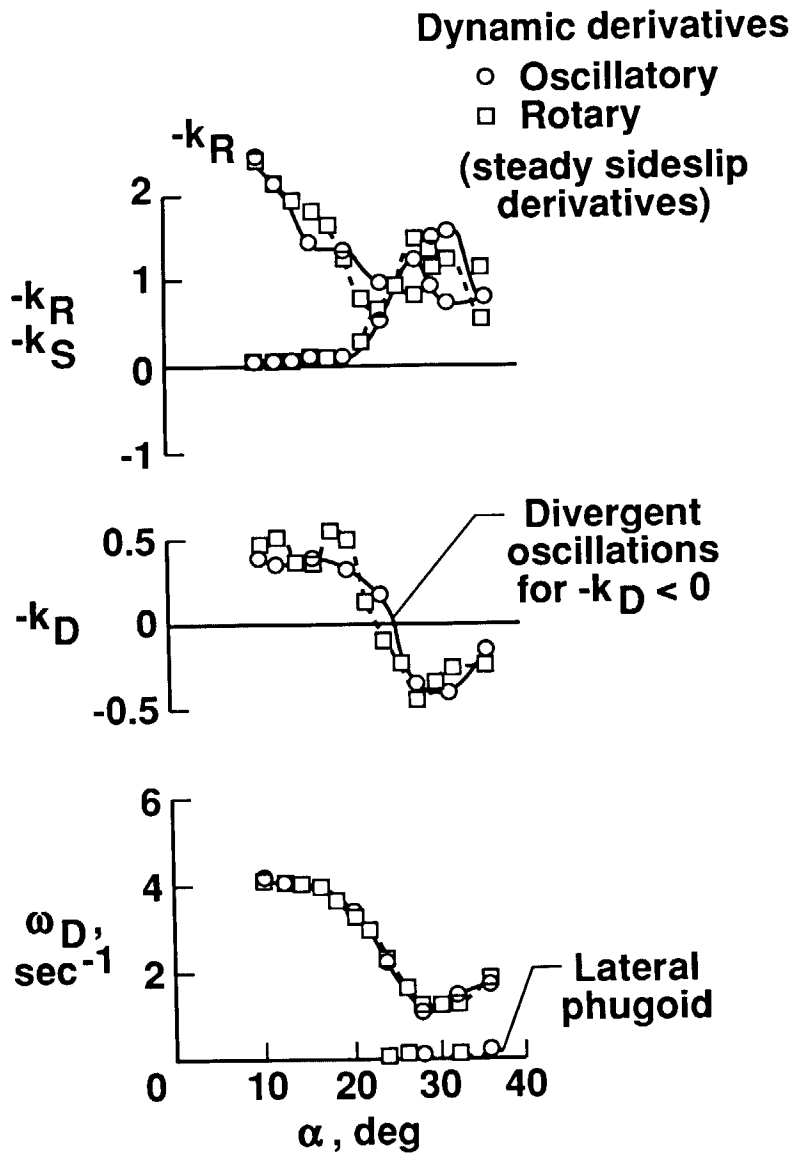

Figure 19. Effect of different dynamic derivatives. Figure taken from reference 4.

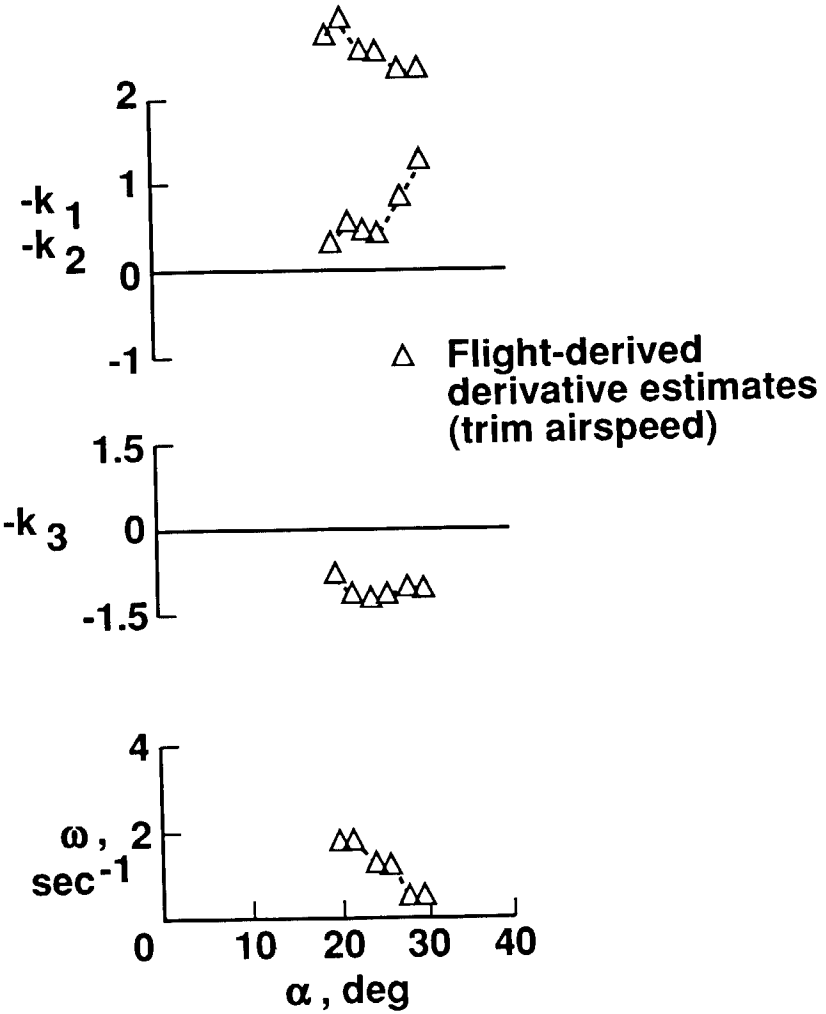

Figure 20. Lateral mode characteristics using derivatives estimated from flight data.

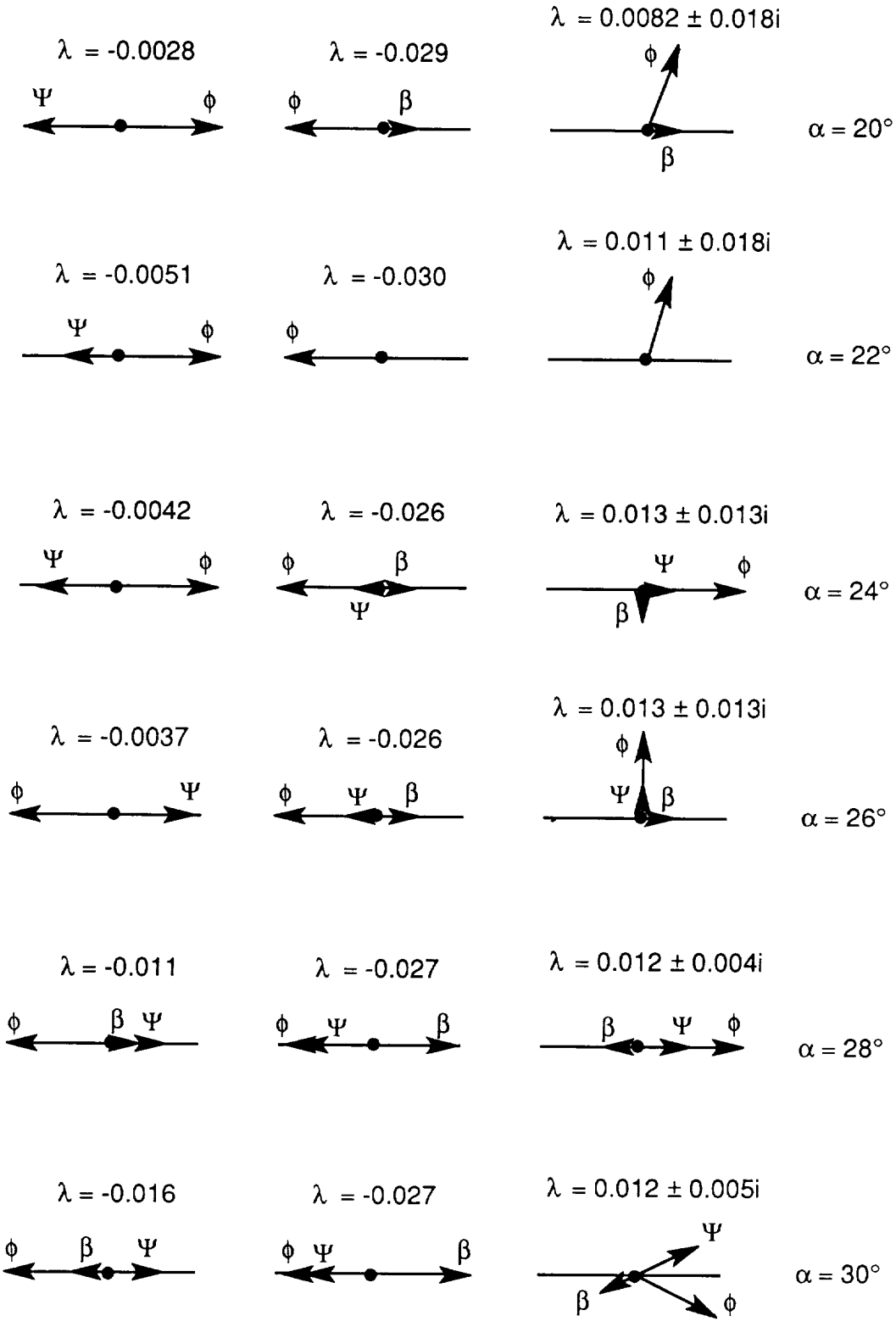

Figure 21. Eigenvectors using derivatives estimated from flight data.

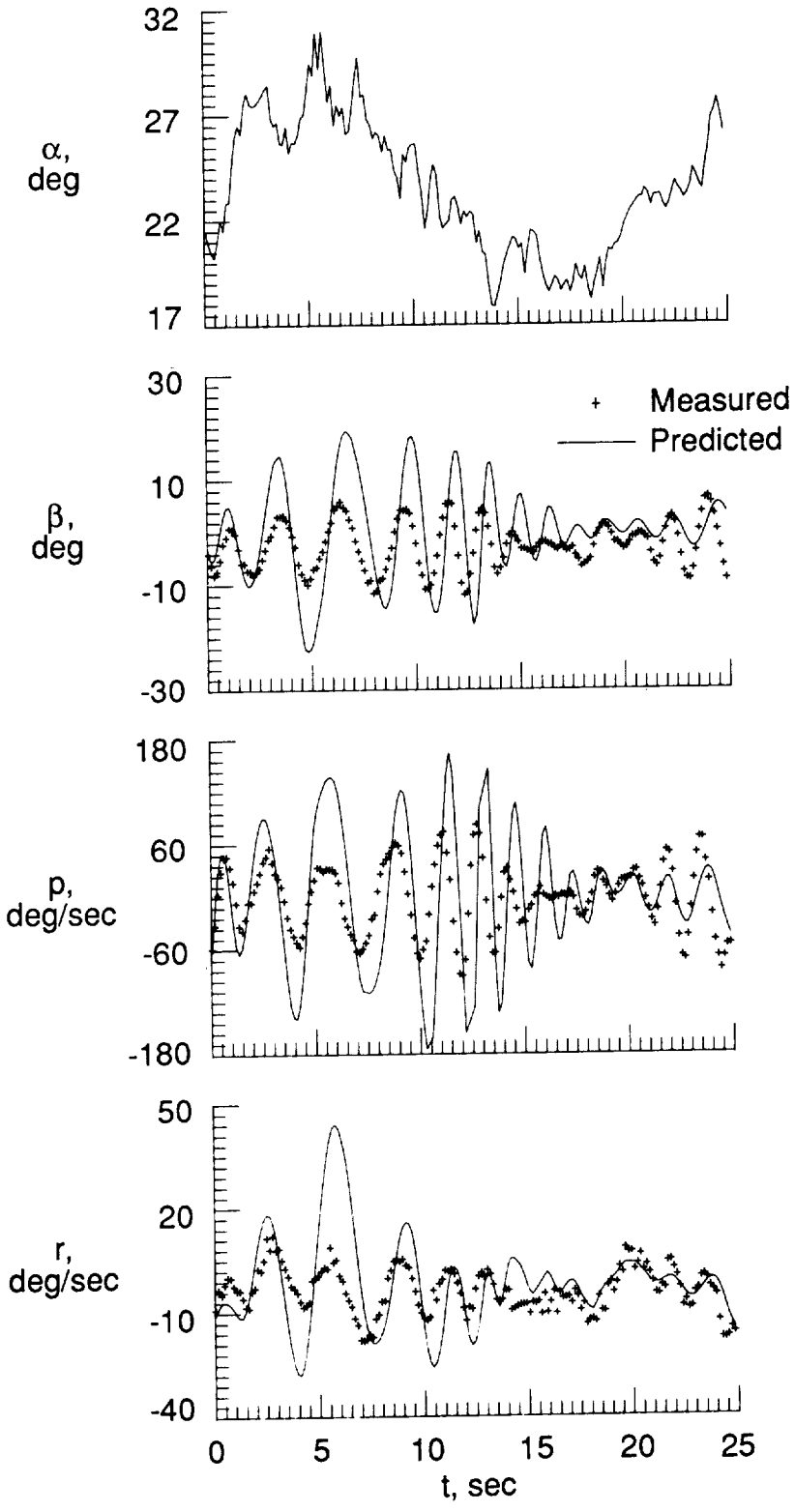

Figure 22. Comparison of measured lateral time histories with those computed from mathematical model of HIRM.

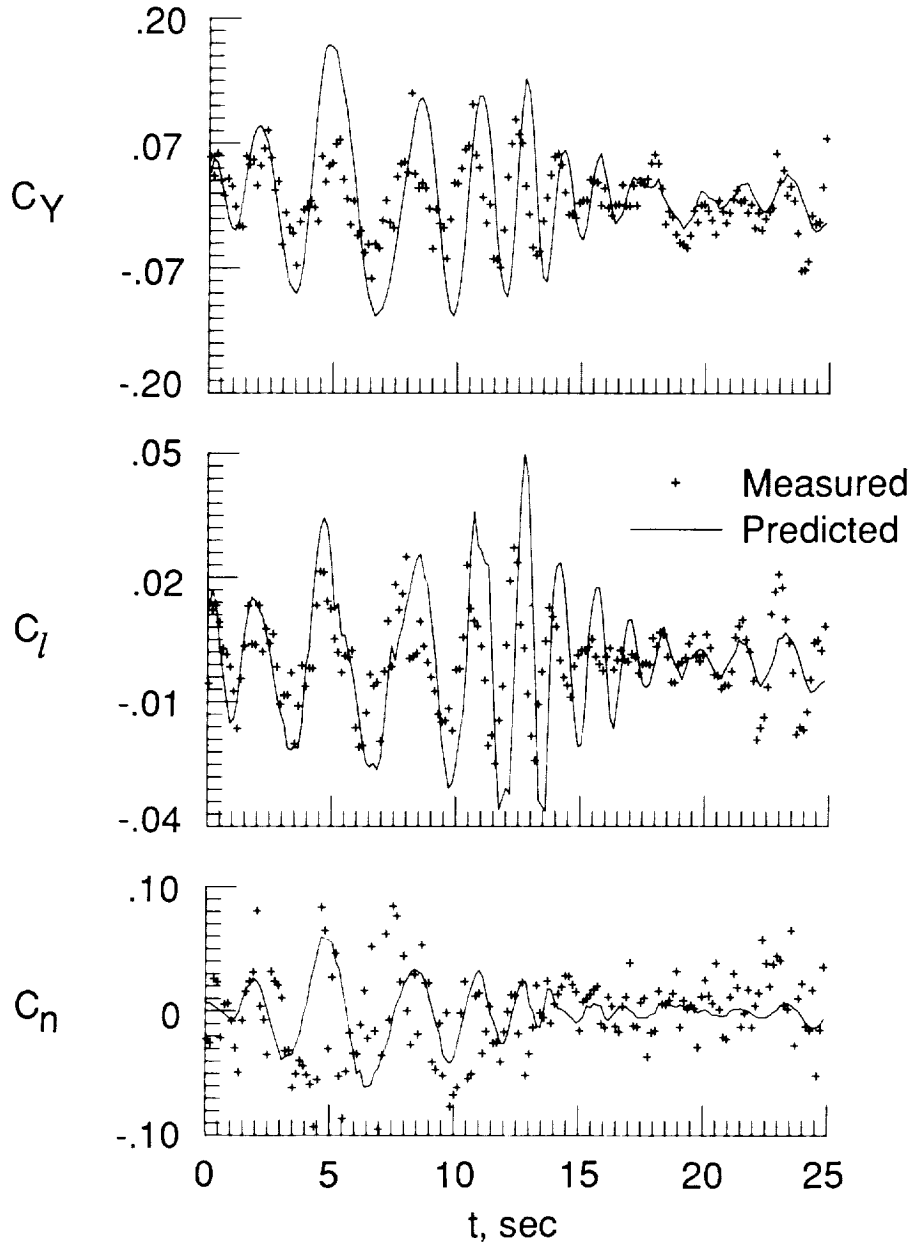

Figure 23. Comparison of measured lateral aerodynamic coefficients with those computed from mathematical model of HIRM.

NASA
National Aeronautics and Space Administration

Report Documentation Page

1. Report No.	2. Government Accession No.	3. Recipient's Catalog No.
NASA TP-2940		

4. Title and Subtitle	5. Report Date
Analysis of Flight Data From a High-Incidence Research Model by System Identification Methods	November 1989
	6. Performing Organization Code
7. Author(s)	8. Performing Organization Report No.
James G. Batterson and Vladislav Klein	L-16571
9. Performing Organization Name and Address	10. Work Unit No.
NASA Langley Research Center Hampton, VA 23665-5225	505-66-01-02
	11. Contract or Grant No.
12. Sponsoring Agency Name and Address	13. Type of Report and Period Covered
National Aeronautics and Space Administration Washington, DC 20546-0001	Technical Paper
	14. Sponsoring Agency Code

15. Supplementary Notes

James G. Batterson: NASA Langley Research Center, Hampton, Virginia.
Vladislav Klein: The George Washington University, Joint Institute for Advancement of Flight Sciences, Langley Research Center, Hampton, Virginia.

16. Abstract

Data partitioning and modified stepwise regression were applied to recorded flight data from a Royal Aerospace Establishment (RAE) high-incidence research model (HIRM). An aerodynamic model structure and the corresponding stability and control derivatives were determined for angles of attack between 18° and 30°. Several nonlinearities in angles of attack and sideslip as well as a unique roll-dominated set of lateral modes were found. All flight-estimated values were compared with available wind-tunnel measurements.

17. Key Words (Suggested by Authors(s))	18. Distribution Statement
System identification Stepwise regression High angle of attack Drop model Partitioning	Unclassified—Unlimited Subject Category 08

19. Security Classif. (of this report)	20. Security Classif. (of this page)	21. No. of Pages	22. Price
Unclassified	Unclassified	49	A03

NASA-Langley, 1989

For sale by the National Technical Information Service, Springfield, Virginia 22161-2171

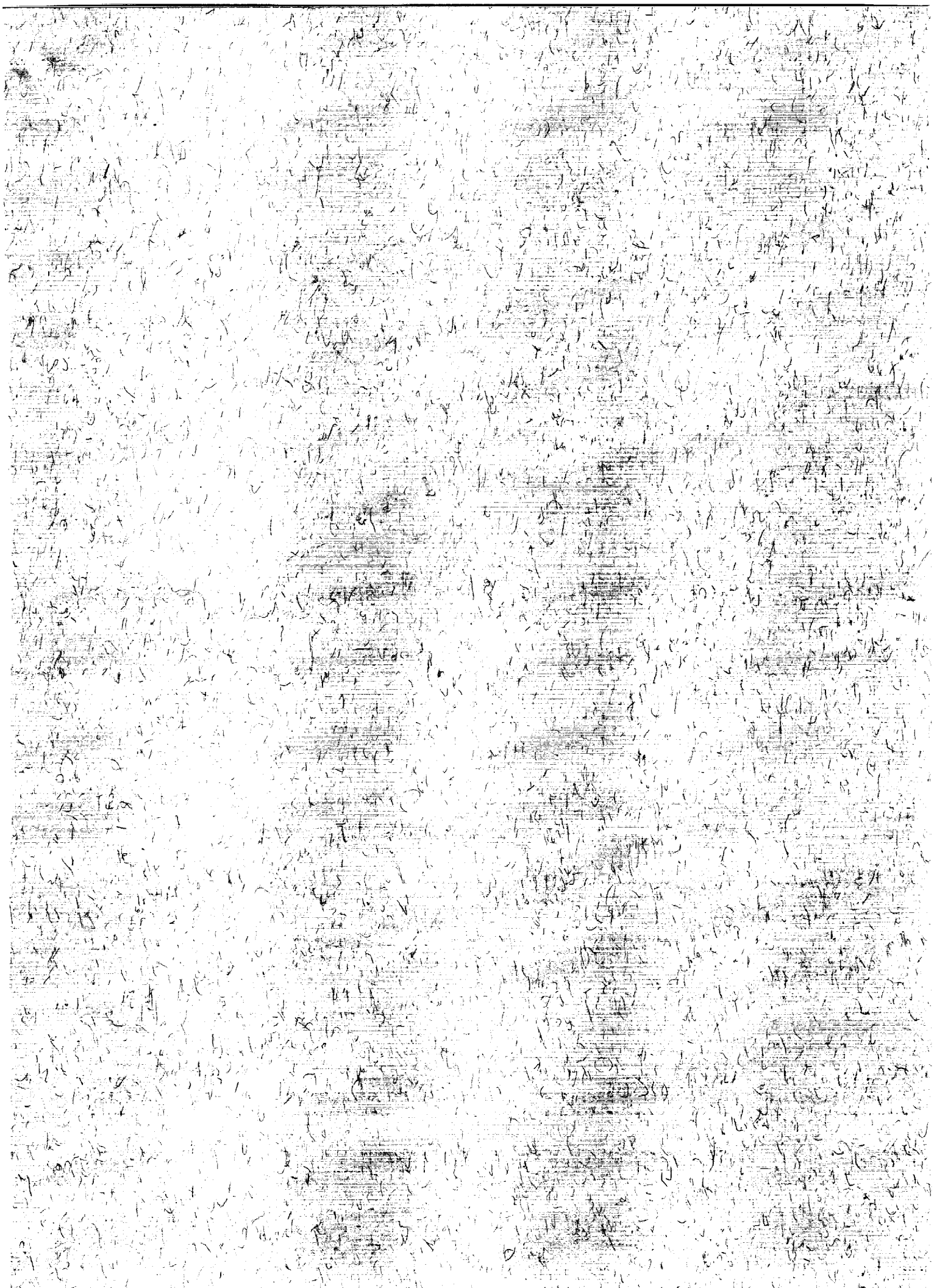

National Aeronautics and
Space Administration
Code NTT-4

Washington, D.C.
20546-0001

Official Business
Penalty for Private Use, $300

BULK RATE
POSTAGE & FEES PAID
NASA
Permit No. G-27

NASA

POSTMASTER: If Undeliverable (Section 158 Postal Manual) Do Not Return